ACS BIO & MED CHEM Au
AN OPEN ACCESS JOURNAL OF THE AMERICAN CHEMICAL SOCIETY

pubs.acs.org/biomedchemau
Article

Chlorophyllase from *Arabidopsis thaliana* Reveals an Emerging Model for Controlling Chlorophyll Hydrolysis

Published as part of ACS Bio & Med Chem Au special issue "2024 Rising Stars in Biological, Medicinal, and Pharmaceutical Chemistry".

Madison Knapp, Minshik Jo, Courtney L. Henthorn, Marley Brimberry, Andrew D. Gnann, Daniel P. Dowling, and Jennifer Bridwell-Rabb*

Cite This: *ACS Bio Med Chem Au* 2024, 4, 353−370
Read Online

ACCESS | Metrics & More | Article Recommendations | Supporting Information

ABSTRACT: Chlorophyll (Chl) is one of Nature's most complex pigments to biosynthesize and derivatize. This pigment is vital for survival and also paradoxically toxic if overproduced or released from a protective protein scaffold. Therefore, along with the mass production of Chl, organisms also invest in mechanisms to control its degradation and recycling. One important enzyme that is involved in these latter processes is chlorophyllase. This enzyme is employed by numerous photosynthetic organisms to hydrolyze the phytol tail of Chl. Although traditionally thought to catalyze the first step of Chl degradation, recent work suggests that chlorophyllase is instead employed during times of abiotic stress or conditions that produce reactive oxygen species. However, the molecular details regarding how chlorophyllases are regulated to function under such conditions remain enigmatic. Here, we investigate the *Arabidopsis thaliana* chlorophyllase isoform *At*CLH2 using site-directed mutagenesis, mass spectrometry, dynamic light scattering, size-exclusion multiangle light scattering, and both steady-state enzyme kinetic and thermal stability measurements. Through these experiments, we show that *At*CLH2 exists as a monomer in solution and contains two disulfide bonds. One disulfide bond putatively maps to the active site, whereas the other links two N-terminal Cys residues together. These disulfide bonds are cleaved by chemical or chemical and protein-based reductants, respectively, and are integral to maintaining the activity, stability, and substrate scope of the enzyme. This work suggests that Cys residue oxidation in chlorophyllases is an emerging regulatory strategy for controlling the hydrolysis of Chl pigments.

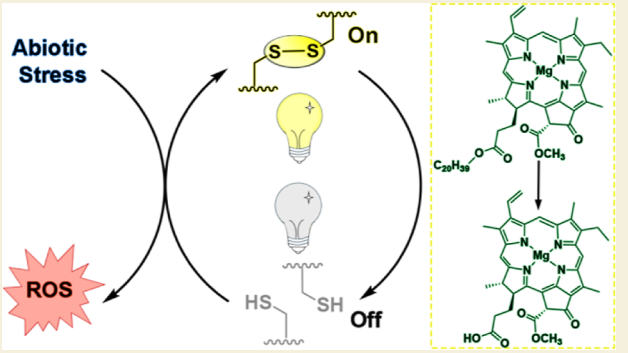

KEYWORDS: *chlorophyll, photosynthesis, photosynthetic pigment, lipase, enzyme catalysis, hydrolase, enzyme kinetics*

INTRODUCTION

Estimates suggest that 10^8 to 10^{12} tons of light-absorbing chlorophyll (Chl) pigments are produced every year by an assortment of organisms to support photosynthesis.[1,2] In this essential biological process, Chl pigments are employed to capture light energy from the sun, which is used to fuel formation of O_2 and chemical energy.[1] The value of Chl to photosynthetic organisms, however, comes with challenges. The same properties that render Chl well suited to absorb light energy also have the potential to adversely impact the health of a photosynthetic organism.[3,4] For example, singlet oxygen ($^1O_2$) can be produced via reaction of an excited triplet state Chl pigment with O_2, and superoxide ($O_2^{\bullet-}$) can be generated by transfer of a leaked electron from the photosynthetic electron transport chain to O_2.[5,6] These O_2-derived molecules, together with peroxide (O_2^{2-}), hydroxyl radicals ($OH^{\bullet}$), and hydrogen peroxide (H_2O_2), are known as reactive oxygen species (ROS). ROS have the ability to oxidatively damage photosynthetic complexes and the plethora of biomolecules found in the cell.[5−7] Therefore, photosynthetic organisms must balance the biosynthesis and degradation of Chl to avoid dangerous levels of pigment production, and must also embrace mechanisms to degrade Chl if aberrantly released from a protective protein home due to environmental stress, disease, or herbivory.[3,4] Beneficially, additional mechanisms also exist to mitigate the potential phototoxic effects of Chl.[8−10] Such defense mechanisms involve a host of chemical and protein-based antioxidants, as well as thioredoxin proteins to resolve the ROS-induced disulfide bonds that can be formed in proteins.[7−10] ROS are also

Received: September 2, 2024
Revised: October 15, 2024
Accepted: October 16, 2024
Published: November 20, 2024

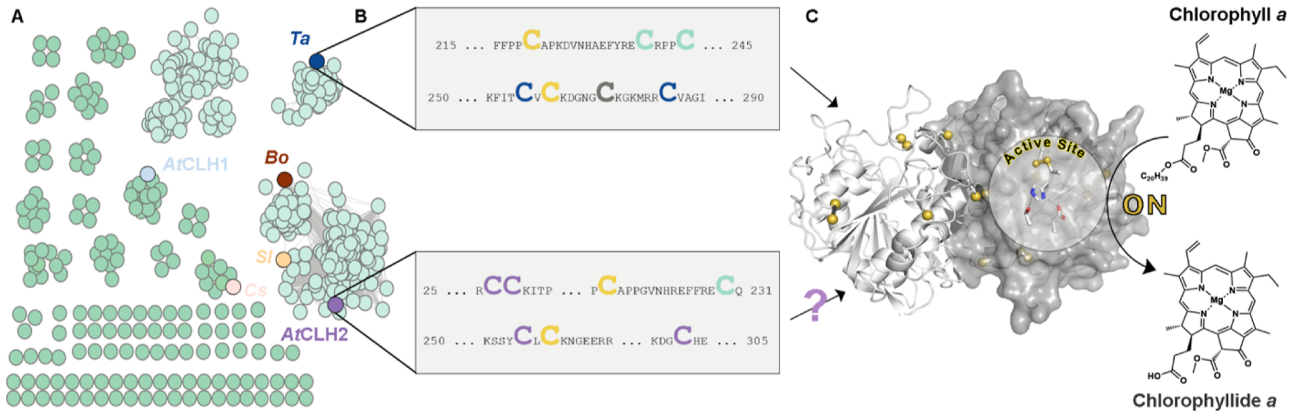

Figure 1. Chlorophyllases catalyze the transformation of chlorophyll (Chl) *a* into chlorophyllide (Chlide) *a* and show variability in the identity of catalytically important Cys residues. (A) A subnetwork of the previously calculated plant sequence similarity network reveals separation of chlorophyllases into groups.[14] Here, the abbreviations *At*, *Bo*, *Sl*, and *Cs* correspond to *A. thaliana*, *Brassica oleracea*, *Solanum lycopersicum*, and *Citrus sinensis*, respectively. These proteins do not contain the same seven Cys residues as the previously investigated *T. aestivum* (*Ta*) chlorophyllase protein. Therefore, these proteins may lack some of the previously observed *Ta*chlorophyllase disulfide bonds. (B) *Ta*chlorophyllase contains seven Cys residues.[14] Five of these Cys residues are used to form an active site disulfide bond (Cys220 and Cys264), an intramolecular disulfide (Cys234 and Cys238), and an intermolecular disulfide bond (Cys270). These Cys residues are highlighted in gold, cyan and gray, respectively. Two additional Cys residues found in the primary sequence are indicated in blue. Despite the importance of these disulfide bonds to the activity and stability of dimeric *Ta*chlorophyllase, this Cys residue architecture is not universally conserved. Therefore, in this work, a plethora of biochemical experiments were performed to understand how the divergent Cys architecture of *A. thaliana* CLH2 (*At*CLH2) impacts catalytic function. *At*CLH2 lacks the equivalent of the Cys residue needed to complete one of the intramolecular disulfide bonds (Cys238) of *Ta*chlorophyllase and also lacks the Cys residue that forms the intermolecular disulfide bond of *Ta*chlorophyllase (Cys270). For *At*CLH2, the Cys residues that align with Cys220 (gold), Cys264 (gold), and Cys234 (cyan) of *Ta*chlorophyllase are highlighted. Four additional Cys residues found in the primary sequence are highlighted in purple. (C) The disulfide rich dimer of *Ta*chlorophyllase[14] is the active form that catalyzes formation of Chlide *a*. The active site is also shown in Figure S1.

well-known signaling molecules that are propagated to facilitate acclimation of photosynthetic organisms to abiotic stress.[7]

Integral to the degradation of Chl *a* is the liberation of the hydrophobic tail from the macrocyclic chlorin scaffold to produce chlorophyllide (Chlide) *a*. This reaction is routinely suggested to be catalyzed by an α/β hydrolase enzyme known as chlorophyllase (Figures 1 and S1).[3,4,11] However, recent reports show that the *A. thaliana* chlorophyllase isoforms, CLH1 (*At*CLH1) and CLH2 (*At*CLH2), are not required for Chl degradation during senescence and are not localized to the chloroplast, an organelle typically considered to house key enzymes from the degradative Chl pathway.[3,12,13] Consistent with these observations and the notion that the *A. thaliana* proteins play a different role in Chl metabolism, several studies have implicated chlorophyllases in the biotic and abiotic stress response.[3,14−17] In particular, the gene encoding *At*CLH1 is known to be induced under conditions that simulate the effects of wounding or pathogen infection.[3,14,15,17] Additionally, the hydrolysis activity of *Triticum aestivum* chlorophyllase (*Ta*-chlorophyllase) has been demonstrated to rely on the presence of disulfide bonds in vitro.[14] More specifically, it has been shown that *Ta*chlorophyllase, which is 47% identical in sequence to *At*CLH1, adopts an α/β hydrolase fold, contains a divalent metal ion binding site, and contains both intramolecular and intermolecular disulfide bonds (Figure 1).[14] Whereas the metal ion does not appear to have an appreciable effect on the activity of *Ta*chlorophyllase, the disulfide bonds impact both the activity and stability of the enzyme. These covalent linkages thus provide a direct mechanism to sense varying environmental stressors that form ROS.[14]

Despite the importance of disulfide bonds to the chemistry of *Ta*chlorophyllase, bioinformatic analyses revealed that outside of the grass family, the Cys residues that make up the disulfide bonds are not universally conserved among annotated chlorophyllases[14] (Figure 1). Rather, there are an abundance of chlorophyllase protein homologues that contain alternative Cys-rich motifs[14] (Figure 1). Due to the importance of these residues to the function of *Ta*chlorophyllase, it is possible that these differences correlate with contrasting levels of activity or divergent roles in Chl metabolism. Indeed, two chlorophyllase homologues from *S. lycopersicum,* contain only four-to-five of the seven *T. aestivum* Cys residues and have been suggested to additionally participate in the degradation of pheophytin *a* (Phein *a*) in vivo.[18] Likewise, chlorophyllase homologues from *C. sinensis* and *B. oleracea*, which contain just four of the *Ta*chlorophyllase Cys residues, are thought to be involved in Chl dephytylation during fruit ripening and postharvest senescence, respectively.[18−21] *At*CLH1 and *At*CLH2 proteins similarly each contain just the equivalent of four of the disulfide-bond forming *T. aestivum* Cys residues. However, as described above, despite this divergent Cys architecture, available data for *At*CLH1 appears to support its role in the *A. thaliana* stress response.[3,15−17] The function of *At*CLH2, on the other hand, remains more mysterious.[3,15−17] To date, *At*CLH2 has been shown to be phylogenetically separated from *At*CLH1,[13] transcriptionally induced in a light-dependent manner in young plant leaves,[22] and a less prominent player, relative to *At*CLH1, in Chl dephytylation in vivo.[12] Nevertheless, other studies have revealed that disruption of the *At*CLH2 encoding gene results in a lower cellular population of Chlide relative to Chl.[23] Based on the noted importance of chlorophyllases to crop growth, produce lifetime, and the growth of photosynthetic organisms,[3,4,24,25] it is paramount to identify how different sequence fingerprints contribute to different noted functionalities.

In this work, we use site-directed mutagenesis, steady-state enzyme kinetic experiments, intact mass spectrometry, dynamic light scattering (DLS), size-exclusion multiangle light scattering

https://doi.org/10.1021/acsbiomedchemau.4c00089
ACS Bio Med Chem Au 2024, 4, 353−370

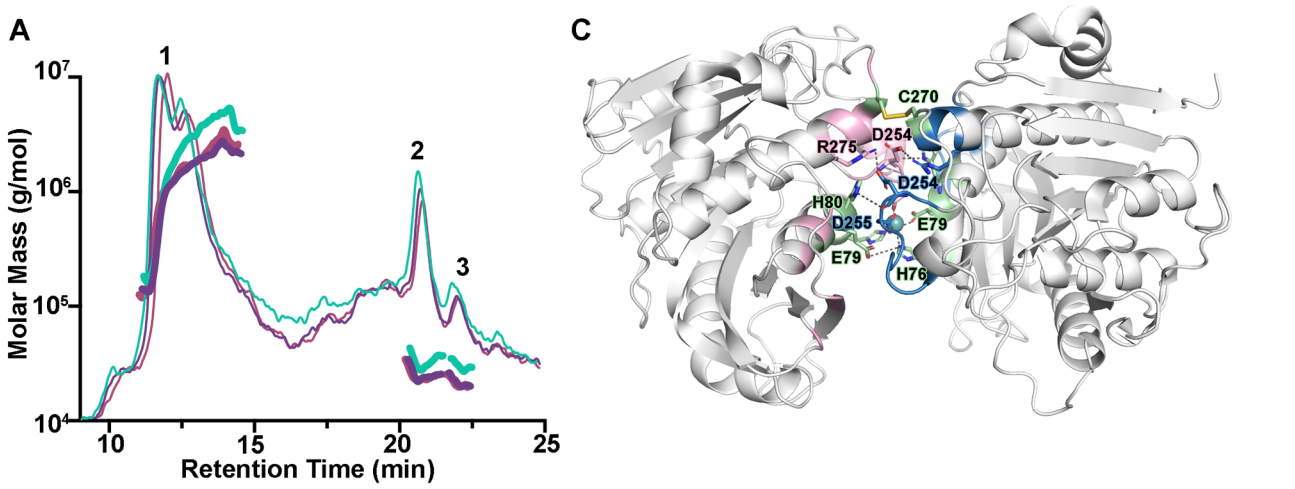

B

```
TaChlase        1 MAAAAPAETMNKSAAGAEVPEAFTSVFQPGKLAVEAIQVDEN--------     42
AtCLH2          1 ---------MSSSSS--------RNAFEDGKYKSNLLTLDSSSRCCKITP     33

TaChlase       43 ---AAPTPPIPVLIVAPKDAGTYPVAMLLHGFFLHNHFYEHLLRHVASHG     89
AtCLH2         34 SSRASPSPPKQLLVATPVEEGDYPVVMLLHGYLLYNSFYSQLMLHVSSHG     83

TaChlase      236 PPCYYLVTKDYGHLDMLDDDAP----KFITCVCKDGNGCKGKMRRCVAGI    281
AtCLH2        232 GPAWHFVAKDYGHLDMLDDDTKGIRGKSSYCLCKNGEE-RRPMRRFVGGL    280
```

Figure 2. *At*CLH2 behaves as a monomeric protein in solution. (A) As evidenced by size-exclusion multiangle light scattering (SEC-MALS), *At*CLH2 exists predominantly as a monomeric species in solution. The molecular weight is denoted here by dark lines whereas light scattering is indicated by fine lines. All three replicates are included in this panel. As detailed in Table 1, peak 1 corresponds to an aggregated protein fraction (approximately 6% of the total protein population) and peaks 2 and 3 correspond to monomeric *At*CLH2 species (approximately 94% of the total protein population). (B) *At*CLH2 shows differences in the identity of residues found at the dimeric interface in *Ta*chlorophyllase. The dimeric interface residues highlighted in this panel were identified using the ePISA server.[27] These residues are highlighted in light gray in the sequence alignment. The residues in bold blue font ligate the divalent metal ion of *Ta*chlorophyllase. The residues shown in bold black font form electrostatic interactions at the interface. Cys270 is in red and forms the intermolecular disulfide bond of *Ta*chlorophyllase. (C) The side chains of residues from the monomeric units that form interactions with residues on the adjacent monomer, or ligate the metal ion (teal sphere) are shown as sticks (see bold residues in panel B). Pink and blue highlighted residues correspond to those from panel B that were identified using the ePISA server[27] in the left and right monomeric units of *Ta*chlorophyllase (PDB: 8FJD[14]), respectively. Residues that are not conserved in AtCLH2 are highlighted in green. Only a portion of the full sequence alignment from Figure S4 is shown in this figure.

(SEC-MALS), and thermal stability measurements to identify how the alternate Cys architecture of *At*CLH2 affects its activity and stability in vitro. Through these experiments, we show that *At*CLH2 exhibits a different oligomeric state than the *Ta*chlorophyllase homologue and contains two disulfide bonds. This protein shows lower hydrolysis activity and is less thermal stable in vitro. Additionally, this work reveals that the disulfide bonds and the activity of *At*CLH2 are sensitive to both small molecule- and protein-based reductants. Therefore, this work contributes to an emerging trend by which α/β hydrolase proteins can be modulated by changes in the primary and quaternary structures and via post-translational modification of Cys residues. Furthermore, it highlights that post-translational modification remains an important regulatory mechanism that governs catalysis in chlorophyllases and emphasizes the importance of studying the sequence-structure−function relationships in this enzyme class.

RESULTS

*At*CLH2 Exists as a Monomer in Solution

To examine the activity of *At*CLH2 in vitro, a codon optimized gene encoding C-terminally His-tagged *At*CLH2 was synthesized and used for overexpression in *Escherichia coli*. *At*CLH2 was thereafter purified using a two-step series of affinity and size exclusion chromatography columns (Figure S2). Based on the latter size-based purification step, it was estimated that purified *At*CLH2 behaves as a monomeric species in solution. This finding is different from the dimeric state observed for *Ta*chlorophyllase in crystallo and using gel filtration purification[14] (Figure S2B).

To further probe the apparent difference in the oligomeric states of *At*CLH2 and *Ta*chlorophyllase in solution, DLS and in-line SEC-MALS experiments were conducted (Figure S3). These experiments revealed that *Ta*chlorophyllase (69 kDa), as predicted based on gel filtration and X-ray crystallography experiments,[14] exists predominantly as a dimer in solution with a hydrodynamic radius (R_h) of 47 Å (Tables S1, S2 and Figure S3A,B). Further screening of protein concentrations in the range of 5−250 μM by DLS demonstrated a consistent R_h value (Figure S3D and Table S3). This value is larger than the calculated R_h (32.6 Å) for the previously published X-ray crystal structure of the dimeric enzyme.[14,26] Interestingly, the SEC-MALS experiments with *At*CLH2 reveal the presence of three species (Figure 2A and Table 1). The two major species, which account for more than 90% of the total protein population, have molar masses that are most consistent with an *At*CLH2 monomer (36 kDa, Figure 2A and Table 1). A third species is also present in the analyzed sample, but it accounts for approximately only 6% of the total protein population, and

https://doi.org/10.1021/acsbiomedchemau.4c00089
ACS Bio Med Chem Au 2024, 4, 353−370

Table 1. SEC-MALS Peaks of *At*CLH2[a]

	peak 1		peak 2		peak 3	
	MW (kDa)	mass fraction (%)	MW (kDa)	mass fraction (%)	MW (kDa)	mass fraction (%)
*At*CLH2-1	1407.3	5.5	32.4	64.1	29.8	30.3
*At*CLH2-2	932.6	6.6	24.3	62.9	21	30.5
*At*CLH2-3	909.4	6.7	23.5	62.8	20.6	30.5
average	1083	6.3	26.7	63.3	23.8	30.4
std. dev.	281	0.7	4.9	0.7	5.2	0.1

[a]This table contains the experimental molecular weights and percent mass fraction for each detected peak. Based on use of the ProtParam tool,[28] the calculated molecular weight of an *At*CLH2 monomer is approximately 36 kDa, whereas the calculated molecular weight of the dimer would be approximately 72 kDa. This data indicates there are two monomeric fractions of *At*CLH2 that likely show subtle differences in tertiary architecture.

corresponds to an aggregated protein fraction (Figure 2A and Table 1). DLS experimental data for this protein reveals a smaller R_h value of 40 Å (Figure S3C and Table S1). Again, this value is similar, albeit larger than the calculated R_h (24.9 Å) for a single protomer of the dimeric *Ta*chlorophyllase structure.[14,26] Perhaps related to these differences in oligomeric state, a Protein Interfaces, Surface and Assemblies (PISA) analysis[27] and sequence alignment reveal that *At*CLH2 has the equivalent of only a number of the 25 dimeric interface residues found in *Ta*chlorophyllase (Figure 2B,C). More precisely, through this analysis, it was determined that *At*CLH2 lacks an equivalent of the *Ta*chlorophyllase residues that form a covalent linkage (Cys270), coordinate a divalent metal ion (His76), and engage in electrostatic interactions at the dimeric interface (Glu79 and His80, Figure 2B,C). To probe the importance of these residues to oligomeric state, three variants of *Ta*chlorophyllase were produced (Table S4 and Figure S4). From this series, it was determined that a triple *Ta*chlorophyllase variant in which His76, Glu79, and Cys270 are mutated into Ser residues, still exists, based on DLS and SEC-MALS experiments, as a dimeric species in solution (Tables S5, S6 and Figures S5, S6). Additional variants that contain either five (H76S/E79S/H80Q/R83L/C270S) or six (H76S/E79S/H80Q/R83L/C270S/G272R) mutations at the interface also have R_h values reminiscent of the dimeric enzyme (Table S7 and Figures S7–S10). These experiments reveal that only focusing on these highlighted residues is not sufficient to convert *Ta*chlorophyllase into a monomeric species that resembles *At*CLH2.

*At*CLH2 Contains Two Disulfide Bonds

As evident from a sequence alignment and AlphaFold[29,30] model, only four of the seven *Ta*chlorophyllase Cys residues (Cys220, Cys234, Cys262, and Cys264) appear to be conserved in *At*CLH2 (Figures 1 and S4). These four Cys residues correspond to Cys216, Cys230, Cys262, and Cys264 in *At*CLH2, and accompany two N-terminal Cys residues (Cys28 and Cys29), as well as a seventh Cys residue (Cys303) that is located in the C-terminal region of the primary sequence (Figure S4B,C). This analysis suggests that *At*CLH2 likely contains only the equivalent of the *Ta*chlorophyllase active site disulfide bond. To confirm this alternate disulfide bond architecture, an investigation into the disulfide bond character of *At*CLH2 was undertaken using wild-type *At*CLH2 and a series of variants (C28S, C29S, C216S, C230S, C262A, C262S, C264S, C303S, C216S/C262S, and C216S/C264S, Table S4 and Figure S11). These variants were created using site-directed mutagenesis and were subsequently expressed and purified using the same methods described for the wild-type enzyme (Table S4 and Figure S11).

Using the wild-type protein and the purified library of *At*CLH2 variants, a series of mass spectrometry experiments were employed to assess the protein samples following treatment with reducing (dithiothreitol (DTT)), oxidizing (H_2O_2), and thiol-labeling agents (iodoacetamide (IAA)). As a baseline for these experiments, it was first determined that the as-purified, wild-type sample of *At*CLH2 is four protons short of its calculated mass (Figure 3A). This mass is not altered by the addition of H_2O_2 to the protein sample but is increased by four protons in the presence of DTT (Figure 3A). These findings are consistent with the presence of two disulfide bonds in the wild-type protein. In agreement, wild-type *At*CLH2 incorporates two to three molecules of IAA per monomer, indicating the presence of just two to three free Cys residues (Figure S12).

Using the same set of mass spectrometry experiments, it was next explored whether one of the identified disulfide bonds in the wild-type enzyme involves the equivalent of the active-site disulfide bond forming Cys residues (Cys216 and Cys264) in *Ta*chlorophyllase. In this endeavor, it was determined that a C264S *At*CLH2 variant is two protons short of the calculated mass (Figure 3B). This mass is increased by the addition of DTT and is decreased by just one proton in the presence of H_2O_2 (Figure 3B). These results, along with IAA labeling experiments, suggest that there is one disulfide bond, rather than two, present in the C264S protein (Figures 3B and S13A). These results also signify that Cys264 is involved in a wild-type *At*CLH2 disulfide bond (Figure 3B). Analysis of the C216S and C216S/C264S variant data is less straightforward (Figure 3C). As-purified, these variants lack a disulfide bond and incorporate high levels of IAA (Figures 3C and S13B,C). Furthermore, unlike that observed with the wild-type and C264S variant, treatment of these samples with H_2O_2 leads to the formation of oxidatively modified protein samples (Figure 3C). These results, reminiscent of that observed in *Ta*chlorophyllase,[14] suggest that replacement of the Cys216 residue (Cys220 in *Ta*chlorophyllase numbering) is destabilizing to the structure of *At*CLH2. Consistent with this theory, an analogous set of experiments also revealed that the C216S/C262S variant lacks a disulfide bond (Figure S13D).

To further verify the presence of a Cys216–Cys264 disulfide bond, a C262S variant was analyzed (Figure S14). The as-purified sample of this variant is two protons short of the calculated mass (Figure S14A). However, based on the fact that this variant can be oxidized to contain a second disulfide bond, it was hypothesized that Cys262 is not part of a linkage in the wild-type enzyme (Figure S14). To confirm this proposal, a complementary variant, C262A was recombinantly expressed and purified (Figure S15A,B). This variant is four protons short of the calculated mass (Figure S15C). Like the C262S variant, the C262A protein can be reduced with DTT and trapped in a state that contains two disulfide bonds (Figure S15C). These results indicate that indeed, Cys262 is not part of a disulfide bond in *At*CLH2. Equivalent experiments performed with C230S and C303S *At*CLH2 variants similarly confirm that Cys230 and Cys303 are also not involved in an *At*CLH2 disulfide bond (Figure S16).

In contrast, following purification, the C28S and C29S variants are each approximately two protons short of the calculated mass (Figure S17). One disulfide bond of these

https://doi.org/10.1021/acsbiomedchemau.4c00089
ACS Bio Med Chem Au 2024, 4, 353–370

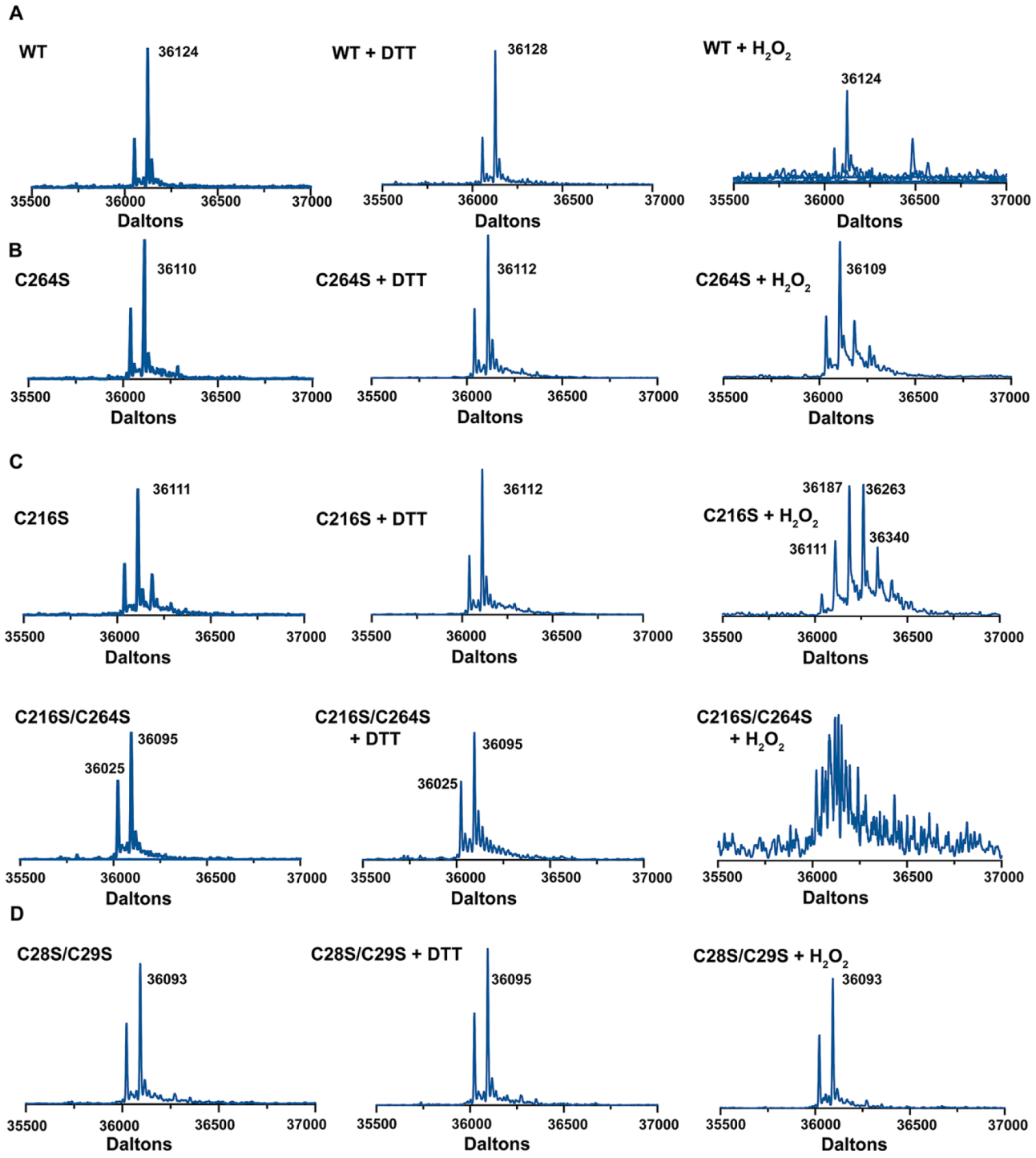

Figure 3. *At*CLH2 contains two intramolecular disulfide bonds. (A) Intact mass spectrometry experiments reveal that the two disulfide bonds found in wild-type *At*CLH2 can be reduced by incubation of the protein with 10 mM DTT. In contrast, as-purified wild-type *At*CLH2 cannot be further oxidized via incubation with H_2O_2. (B) In the C264S *At*CLH2 variant, one disulfide bond can be reduced. One proton is lost from this variant following treatment with H_2O_2. (C) The C216S and C216S/C264S variants do not purify with intact disulfide bonds and are not susceptible to complete reduction with DTT. These variants unlike the wild-type and C264S variant are oxidatively modified following exposure to H_2O_2. (D) The C28S–C29S *At*CLH2 double variant purifies with just one intact disulfide bond. Whereas this bond is susceptible to reduction with DTT, the as-purified protein cannot be further oxidized with H_2O_2. The masses for the wild-type, single, and double variant proteins are 36,128, 36,112, and 36,095 Da, respectively.

variants is reduced by the addition of DTT, but neither of these variants is further oxidized with H_2O_2 (Figure S17). These results suggest that both of these residues are involved in an *At*CLH2 disulfide bond. To provide additional support for this conclusion, a C28S/C29S double variant of *At*CLH2 was recombinantly expressed, purified, and investigated using mass spectrometry (Table S4, Figures 3D and S18). This variant purifies with one disulfide bond that is reducible via incubation with DTT (Figure 3D). As expected, based on mutation of the N-terminal Cys residues and the presence of one disulfide bond,

https://doi.org/10.1021/acsbiomedchemau.4c00089
ACS Bio Med Chem Au 2024, 4, 353−370

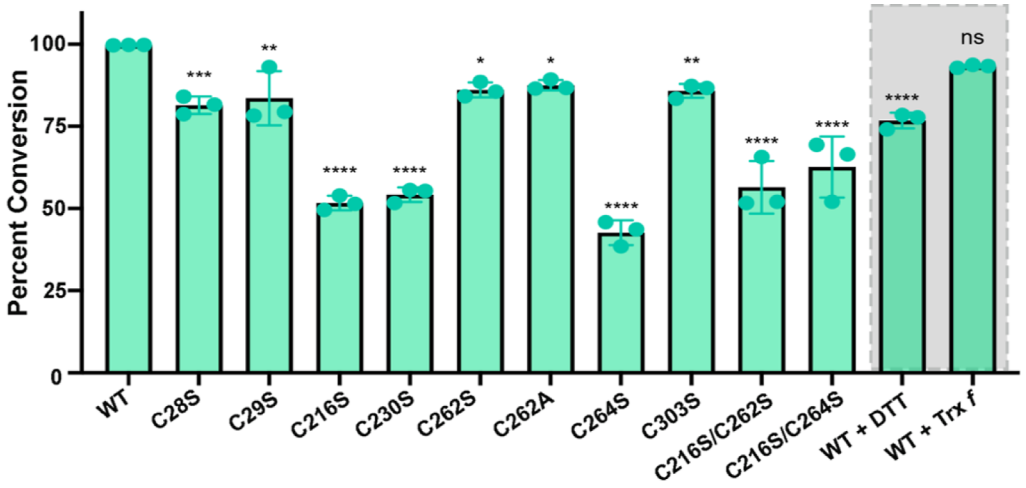

Figure 4. The Cys variants of *At*CLH2 are impaired in their ability to hydrolyze Chl *a*. Here, HPLC was used to detect the amount of Chlide *a* produced following a 35 min incubation of 5 μM *At*CLH2 with 500 μM of Chl *a*. As observed with the Cys variants, treatment of *At*CLH2 with DTT leads to reduced activity (bars on right in the box). In contrast, treatment with Trx *f* has no appreciable impact on the hydrolysis activity of *At*CLH2 (bars on right in the box). In this figure, data were measured using $n = 3$ independent experiments and are presented as the mean value ± SD of these measurements. In this figure, ****$p < 0.0001$, ***$p < 0.001$, **$p < 0.01$, and *$p < 0.1$, indicating significant difference from the mean values of wildtype *At*CLH2 for each respective variant, as determined from an ordinary one-way ANOVA Tukey analysis.

Table 2. Summary of Kinetic Parameters for Wild-Type and Variant *At*CLH2 and *Ta*chlorophyllase Proteins[a]

Protein	K_M (μM)	k_{cat} (sec^{-1})	k_{cat} / K_M (M^{-1} sec^{-1})
*Ta*chlorophyllase (Chl *a*)*	46 ± 6*	8.9 ± 0.5*	230,000 ± 40,000
H76S/E79S/C270S *Ta*chlorophyllase	220 ± 50	7.5 ± 0.9	34,000 ± 9,000
H76S/E79S/H80Q/R83L/C270S *Ta*chlorophyllase	110 ± 30	0.65 ± 0.08	5,900 ± 2,000
H76S/E79S/H80Q/R83L/C270S/G272R *Ta*chlorophyllase	32 ± 7	2.1 ± 0.2	67,000 ± 16,000
*At*CLH2 (Chl *a*)	46 ± 9	1.3 ± 0.1	28,000 ± 6,000
*At*CLH2 (Chl *b*)	109 ± 19	1.5 ± 0.1	14,000 ± 3,000
*At*CLH2 (Phein *a*)	59 ± 9	1.02 ± 0.05	17,000 ± 3,000
*At*CLH2 (Bchl *a*)	89 ± 18	0.46 ± 0.03	5,100 ± 1,000
C28S	62 ± 13	1.9 ± 0.1	31,000 ± 7,000
C29S	42 ± 13	1.6 ± 0.2	38,000 ± 13,000
C216S	29 ± 9	0.71 ± 0.06	24,000 ± 8,000
C264S	22 ± 7	0.87 ± 0.07	40,000 ± 13,000
C216S/C264S	39 ± 12	0.90 ± 0.09	23,000 ± 7,000
C230S	35 ± 6	0.48 ± 0.02	14,000 ± 2,000
C262S	40 ± 20	1.1 ± 0.2	28,000 ± 15,000
C262A	30 ± 8	1.3 ± 0.1	43,000 ± 12,000
C303S	64 ± 8	2.1 ± 0.1	33,000 ± 4,000
C216S/C262S	23 ± 11	0.62 ± 0.06	27,000 ± 13,000
S138A	29 ± 10	0.15 ± 0.02	5,200 ± 2,000
S134A/S138A	12 ± 3	0.12 ± 0.01	10,000 ± 3,000
Y65F	84 ± 18	0.32 ± 0.03	3,800 ± 900
Y68F	49 ± 14	1.6 ± 0.2	33,000 ± 10,000
Y65F/Y68F	32 ±11	0.94 ± 0.1	29,000 ± 11,000

[a]In this table, Chl *a* was used as the substrate of the wild-type and variant *At*CLH2 proteins unless otherwise noted. *This kinetic data is from previously published work.[14] Blue shades are used to highlight disulfide bond forming Cys residues in *At*CLH2 and yellow is used to highlight variants that were made to assess the importance of catalytic residues.

this variant is not susceptible to oxidation by H_2O_2, but can be labeled with IAA (Figures 3D and S19). In total, these results indicate that two disulfide bonds are present in wild-type *At*CLH2. One disulfide bond is formed between Cys216 and Cys264, and a second is formed between Cys28 and Cys29.

Variants of *At*CLH2 and *Ta*chlorophyllase Exhibit Altered Catalytic Activity

To evaluate whether the two identified disulfide bonds are important to the hydrolysis activity of *At*CLH2, a high performance liquid chromatography (HPLC)-based method was designed to separate Chl *a* from Chlide *a* (Figures S20 and S21). In these experiments, it was determined that whereas the

https://doi.org/10.1021/acsbiomedchemau.4c00089
ACS Bio Med Chem Au 2024, 4, 353−370

Table 3. Melting Temperatures Measured for the Proteins and Variants Investigated in This Work[a]

Protein	Thermal Shift T_m (°C)	ΔT_m (°C)
WT *Ta*chlorophyllase*	74.8 ± 0.8*	-
H76S/E79S/C270S	64.4 ± 1.2	-10.4
*Ta*chlorophyllase	86.1 ± 0.1	+11.3
H76S/E79S/H80Q/R83L/C270S	61.2 ± 1.4	-12.8
*Ta*chlorophyllase	83.9 ± 0.1	+9.1
H76S/E79S/H80Q/R83L/C270S/G272S	60.3 ± 0.1	-14.5
*Ta*chlorophyllase	85.6 ± 0.1	+10.8
WT *At*CLH2	59.4 ± 0.3	-
C28S	59.2 ± 0.2	-0.2
C29S	59.7 ± 0.3	+0.3
C28S/C29S	56.8 ± 0.5	-2.6
C216S	49.1 ± 0.1	-10.3
C264S	56.5 ± 0.7	-2.9
C216S/C264S	48.7 ± 0.6	-10.7
C230S	58.1 ± 0.7	-1.3
C262S	61.3 ± 1.0	+1.9
C262A	61.3 ± 0.4	+1.9
C303S	59.0 ± 1.1	-0.4
C216S/C262S	48.2 ± 0.3	-11.2
A234C	57.1 ± 0.1	-2.3
W235C	55.4 ± 0.4	-4.0
E269C	57.3 ± 0.2	-2.1
S138A	58.0 ± 0.2	-1.4
S135A/S138A	59.8 ± 0.3	0.4
Y67F	59.0 ± 0.8	-0.4
Y70F	58.7 ± 0.3	-0.7
Y67F/Y70F	60.2 ± 0.1	+0.8
5 mM DTT	50.5 ± 0.6	-8.9
5 mM β-mecaptoethanol	57.9 ± 0.3	-1.5
5 mM TCEP	55.5 ± 0.2	-3.9
5 mM oxidized glutathione (GSSG)	59.8 ± 0.2	0.4
5 mM reduced glutathione (GSH)	62.5 ± 0.2	3.1
15 μM H_2O_2	59.8 ± 0.5	0.4

[a]*This T_m data is from previously published work.[14] The ΔT_m for the *Ta*chlorophyllase variants are calculated relative to wild-type *Ta*chlorophyllase whereas all ΔT_m for the *At*CLH2 variants are calculated relative to wild-type *At*CLH2. Blue shades are used to highlight disulfide bond forming Cys residues in *At*CLH2. Yellow and pink shades are used to highlight catalytic residue variants and added chemical reductants/oxidants, respectively.

C262A variant does not show a significant deviation in its activity profile relative to the wild-type enzyme, all of the Cys-to-Ser *At*CLH2 variants are impaired in their ability to hydrolyze Chl *a* (Figures 4 and S22). Of these variants, the C216S, C230S, C264S, C216S/C262S, and C216S/C264S proteins show the largest decrease in hydrolysis activity (Figures 4 and S22). Incubation of DTT with wild-type *At*CLH2 results in reduction of the two aforementioned disulfide bonds, and correspondingly leads to a decreased level of activity (Figures 3A, 4, and S23). This decrease is similar to that observed with the C216S, C230S, C264S, C216S/C262S, and C216S/C264S *At*CLH2 variants (Figures 4 and S22, S23).

To further analyze the activity of the *At*CLH2 variants, the steady state kinetic parameters for Chl *a* dephytylation were measured (Table 2 and Figure S24). With Chl *a* as a substrate, wild-type *At*CLH2 shows a k_{cat} value of 1.3 ± 0.1 s^{-1} and a K_M value of 46 ± 9 μM (Table 2 and Figure S24A). As observed in the activity assays described above, the measured kinetic parameters and overall catalytic efficiencies of the C28S, C29S, C262S, C262A, and C303S variants, are relatively similar to those measured for the wild-type enzyme (Table 2 and Figure S24B−F). These parameters fall within a range of values reported for other chlorophyllase homologues that have been assayed in lysate or as partially purified enzymes from plant tissue.[31] However, the catalytic efficiency of *At*CLH2 (28,000 ± 6000 M^{-1} s^{-1}) is remarkably reduced relative to that measured for *Ta*chlorophyllase (230,000 ± 40,000 M^{-1} s^{-1}).[14] The C216S, C230S, C264S, C216S/C262S, and C216S/C264S *At*CLH2 variants, on the other hand, each showcase lower k_{cat} and K_M values than the wild-type enzyme, and therefore exhibit a wide range of calculated catalytic efficiencies (Table 2 and Figure S24G−K). These results show that overall, and analogous to that observed in *Ta*chlorophyllase, an intact Cys216−Cys264 disulfide bond is critical for the hydrolysis activity of *At*CLH2 (Table 2). On the contrary, it seems that the presence of the distinctive N-terminal disulfide bond does not have an appreciable impact on catalysis (Table 2).

https://doi.org/10.1021/acsbiomedchemau.4c00089
ACS Bio Med Chem Au 2024, 4, 353−370

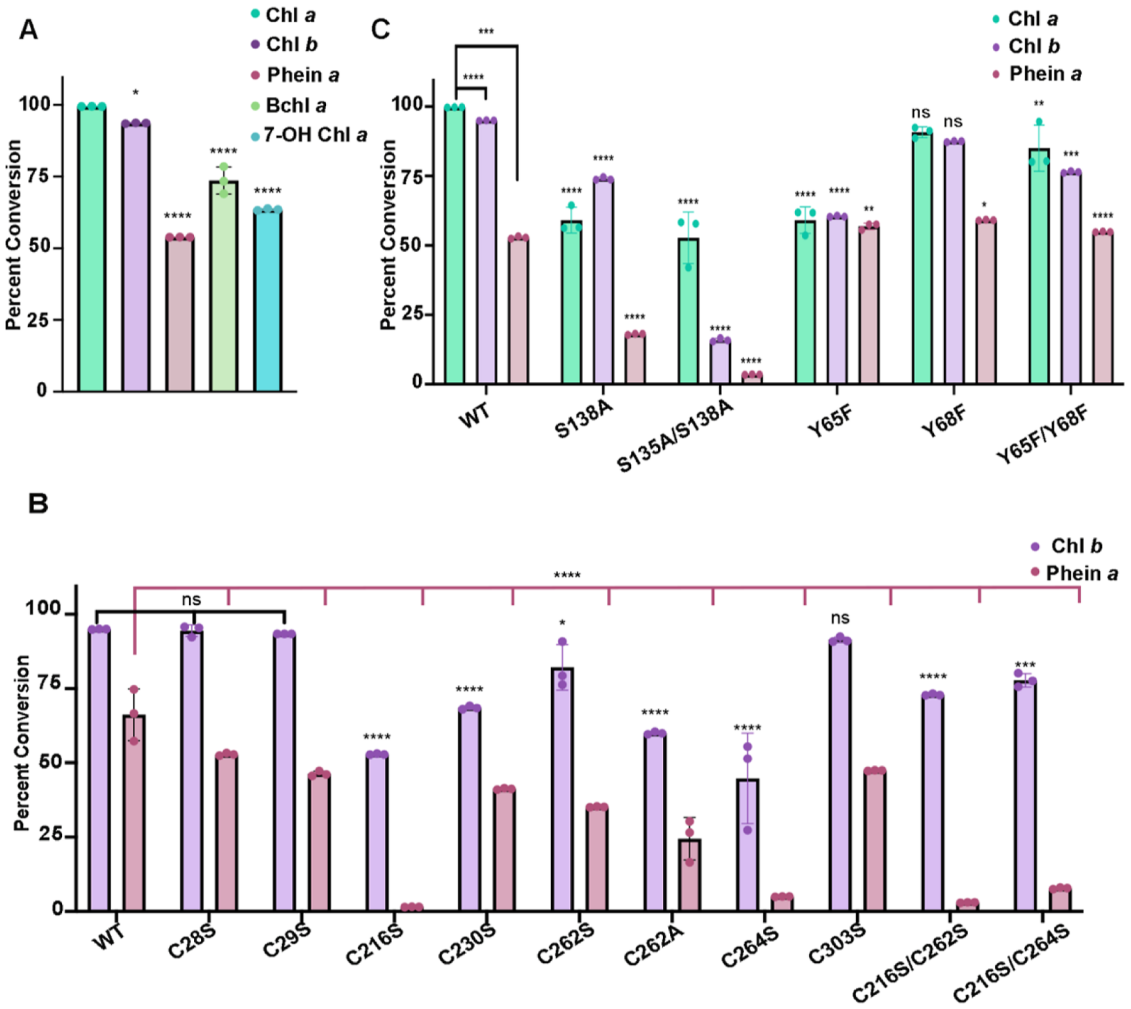

Figure 5. *At*CLH2 dephytylates a diverse set of pigment substrates. (A) An HPLC assay was used to measure the ability of *At*CLH2 to transform pigment substrates, Chl *a*, Chl *b*, Phein *a*, Bchl *a*, and 7-hydroxymethyl (7-OH) Chl *a*, into their tail-free counterparts. In this panel, product formation was measured following a 35 min incubation of 2.5 μM *At*CLH2 with 250 μM pigment substrate. For this experiment, Chl *a* was almost completely consumed by the wild-type enzyme (meaning that the limit of detection was approached for accurate measurement of the amount of substrate consumed). (B) The hydrolysis activity of wild-type *At*CLH2 and its Cys-to-Ser variants was assessed with Chl *b* and Phein *a* substrates. (C) Variants of *At*CLH2 exhibit diminished catalytic activity and altered substrate specificities. The wild-type data shown in this panel with Chl *b* and Phein *a* substrates is reproduced here from panel B and the Chl *a* substrate data is reproduced here from Figure 4 for clarity. For panels B and C, HPLC was used to detect the amount of product formed following a 35 min incubation of 5 μM *At*CLH2 or *At*CLH2 variant with 500 μM of pigment substrate. In this figure, for all panels data were measured using $n = 3$ independent experiments and are presented as the mean value ± SD of these measurements. In this figure, ****$p < 0.0001$, ***$p < 0.001$, **$p < 0.01$, *$p < 0.1$, and indicating significant difference from the mean values of wild type *At*CLH2 for each respective pigment, as determined from an ordinary one-way ANOVA Tukey analysis.

To investigate the origin of the decreased hydrolysis activity of *At*CLH2 relative to *Ta*chlorophyllase, the steady state kinetic parameters for each of the three *Ta*chlorophyllase variants were measured using a Chl *a* substrate and previously described methods[14,31] (Table 2 and Figure S25). From this series of experiments, it was determined that the introduced residue changes have a negative impact on the catalytic efficiencies of the variants. In particular, relative to the wild-type enzyme, the H76S/E79S/C270S *Ta*chlorophyllase variant exhibits an approximate 5-fold increase in K_M and a moderate decrease in k_{cat} (Table 2 and Figure S25A). The H76S/E79S/H80Q/R83L/C270S also has an inflated K_M value of 110 ± 30 μM and a decreased k_{cat}. In the case of this variant, however the k_{cat} is approximately 14-times lower than that measured with the wild-type enzyme (Table 2 and Figure S25B). The H76S/E79S/H80Q/R83L/C270S/G272R variant, based on catalytic efficiency, is the least impacted by the residue changes. That being said, this variant still exhibits a 4-fold decrease in k_{cat} relative to the wild-type enzyme (Table 2 and Figure S25C). These results collectively suggest that the dimeric architecture of *Ta*chlorophyllase is important to its hydrolysis activity.

To investigate whether the lack of the "extra" *Ta*chlorophyllase disulfide bonds may also impact the amount of observed activity in *At*CLH2, an attempt was made to rationally engineer an additional disulfide bond into *At*CLH2.[11] For this approach, three protein variants of *At*CLH2 (A234C, W235C, and E269C) were designed, expressed, and purified (Table S4 and Figure S26). These variants were made because it was anticipated that Ala234 and Trp235 may correspond to the location of Cys238 in *Ta*chlorophyllase, and that Glu269 would likely assume a similar position in the structure to Cys270 (Figure S4). However, none of these variants contain more than two disulfide bonds, or show improved activity relative to the wild-type enzyme (Figures S27 and S28). Rather, these variants

https://doi.org/10.1021/acsbiomedchemau.4c00089
ACS Bio Med Chem Au 2024, 4, 353−370

each showcase significantly lower activity than wild-type *At*CLH2. These results highlight, that consistent with our inability to manipulate the oligomeric state of *Ta*chlorophyllase, at this point, we are also unable to rationally alter the quaternary architecture of *At*CLH2. Therefore, it is expected that the monomeric protein scaffold of *At*CLH2 has distinct differences relative to that of the *T. aestivum* homologue.

Variants of *At*CLH2 and *Ta*chlorophyllase Showcase Differences in Thermal Stability

As previous work indicates that the active site and intermolecular disulfide bonds of *Ta*chlorophyllase are important for enzyme stability,[14] protein thermal shift experiments were used to probe the influence of the Cys residues on the stability of *At*CLH2 (Table 3). For comparison purposes, it was first determined that the melting temperature (T_m) of wild-type *At*CLH2 is 59.4 ± 0.3 °C (Table 3 and Figure S29). For the majority of *At*CLH2 Cys-to-Ser variants, no notable change in T_m is detectable (Table 3 and Figure S29A). However, a striking, and greater than 10 °C decrease in thermal stability is evident for the C216S, C216S/C262S, and C216S/C264S *At*CLH2 variants (Table 3 and Figure S29A). A similar ΔT_m of −8.9 °C is observed for the DTT-treated sample of wild-type *At*CLH2 (Table 3 and Figure S29B). Albeit less substantial than measured with the DTT-treated or the C216S variant, the C264S and C28S/C29S variants also have decreased T_m values relative to the wild-type enzyme (ΔT_m of −2.6 to −2.9 °C, Table 3 and Figure S29A). These measurements are consistent with the idea that disulfide bonds stabilize protein structure by reducing flexibility of the unfolded and folded forms of the protein. Perhaps as expected, based on the above-described activity data, the A234C, W235C, and E269C variants of *At*CLH2 each show a decreased thermal stability relative to the wild-type enzyme (Table 3 and Figure S29C). These results suggest that these variants introduce destabilizing structural perturbations, which again is inconsistent with the insertion of an extra disulfide bond (Table 3 and Figure S29C). Collectively, these differential scanning fluorimetry experiments confirm that comparable to *Ta*chlorophyllase, the *At*CLH2 disulfide bonds are important to maintaining protein architecture at increasing temperatures.

Notably, however, the T_m of wild-type *At*CLH2 is significantly lower than that previously measured for *Ta*chlorophyllase[14] in an equivalent experiment (74.8 ± 0.8 °C, Table 3).To investigate the molecular underpinnings of this difference, the thermal stabilities of the *Ta*chlorophyllase interface variants were also measured. Here, it was determined that unlike the wild-type enzyme, two distinct values are measurable for each of these variants (Table 3 and Figure S30). We hypothesize that these values correspond to two individual events. First, the noncovalently attached dimer breaks apart, and second the tertiary architecture of the monomeric units unfold. As evidenced by the incremental decrease in the T_m of the first unfolding event for the triple, quintuple, and sextuple variants, this data suggests that as mutations are made at the interface, the dimeric quaternary architecture is weakened (Table 3 and Figure S30). This bimodal unfolding scheme contrasts that observed with the wild-type enzyme for which we predict the covalent attachment of monomeric units results in the quaternary and tertiary structures being concurrently disrupted (Figure S30).

*At*CLH2 Variants Exhibit Altered Substrate Preferences

*Ta*chlorophyllase exhibits a broad substrate scope in vitro, meaning that it can accept and hydrolyze a myriad of photosynthetic pigments, including Chl *b*, Phein *a*, bacteriochlorophyll (Bchl) *a*, and 7-hydroxymethyl Chl *a*.[14] To evaluate whether *At*CLH2 similarly performs chemistry on these molecules, the same activity assays described above, were used to demonstrate that wild-type *At*CLH2 also accepts and hydrolyzes Chl *b*, Phein *a*, Bchl *a*, and 7-hydroxymethyl Chl *a* substrates (Table 2, Figures 5A and S31−S37). When *At*CLH2 is provided with a Chl *b* substrate, a near doubling in the K_M value is detectable with only minor changes being measurable with respect to the k_{cat} (Table 2 and Figure S37A). In contrast, despite the observed K_M values with a Phein *a* substrate resembling that measured with a Chl *a* substrate, the k_{cat} is approximately 80% of that observed with the wild-type enzyme and Chl *a* (Table 2 and Figure S37C). For Bchl *a*, the K_M value is nearly double that observed with Chl *a*, and the k_{cat} value is lower than that measured with any other tested pigment (Table 2 and Figure S37B). These values equate to a markedly reduced catalytic efficiency. Similar kinetic experiments were not performed with 7-hydroxymethyl Chl *a* due to the limited amount that can be synthesized. Nevertheless, this molecule, was determined to be turned over to a greater extent than Phein *a* (Figures 5A and S35).

Each of the Cys variants of *At*CLH2 also has the inherent ability to hydrolyze Chl *b*. For this substrate, the trend is relatively similar to that observed with Chl *a*. Namely, the C216S, C230S, C262A, C264S, C216S/C262S, and C216S/C264S variants have the lowest observed levels of dephytylation (Figures 5B and S38). With regard to the metal-free derivative, Phein *a*, all of the Cys variants show significant impairment in hydrolysis activity (Figures 5B and S39). In fact, the activity of the C216S, C264S, C216S/C262S, and C216S/C264S variants is so low, it is almost undetectable in the HPLC-based assay (Figures 5B and S39). This result is intriguing because it suggests that the introduced flexibility into the enzyme by removal of the stabilizing disulfide bonds, makes the scaffold incompatible with Phein *a*, the least planar option of the tested suite of pigment substrates (Figure S31).

An additional investigation was undertaken to understand whether some of the previously identified catalytic residues in *Ta*chlorophyllase are important to the activity of *At*CLH2. Specifically, the impact of mutating residues found in the canonical catalytic motifs was interrogated (Figure S1). Typically, three residues, or a catalytic triad of Ser, His, and Asp residues, are employed to facilitate the hydrolysis reaction. Additionally, the backbone of two residues is needed to form the oxyanion hole and stabilize the negative charge of the formed tetrahedral intermediate. In *Ta*chlorophyllase, Ser145 serves as the nucleophile for the hydrolysis reaction. The equivalent of this residue in *At*CLH2 is Ser138, and as expected, is found in the canonical G−X−S−X−G−X_{small} sequence motif that is characteristic of other α/β hydrolase enzymes[14,32] (Figure S4). As observed in *Ta*chlorophyllase, the S138A variant of *At*CLH2 retains hydrolysis activity (Table 2 and, Figures 5C and S40, S41). However, the activity with a Chl *a* substrate is significantly decreased and the measured k_{cat} of the hydrolysis reaction is approximately 10-times lower relative to the wild-type enzyme (Table 2, Figures 5C and S41). The S138A variant also demonstrates a slight preference for a Chl *b* pigment over Chl *a* suggesting that it may play an important role in dictating the substrate selectivity of *At*CLH2 (Figures 5C and S41B). As the

https://doi.org/10.1021/acsbiomedchemau.4c00089
ACS Bio Med Chem Au 2024, 4, 353−370

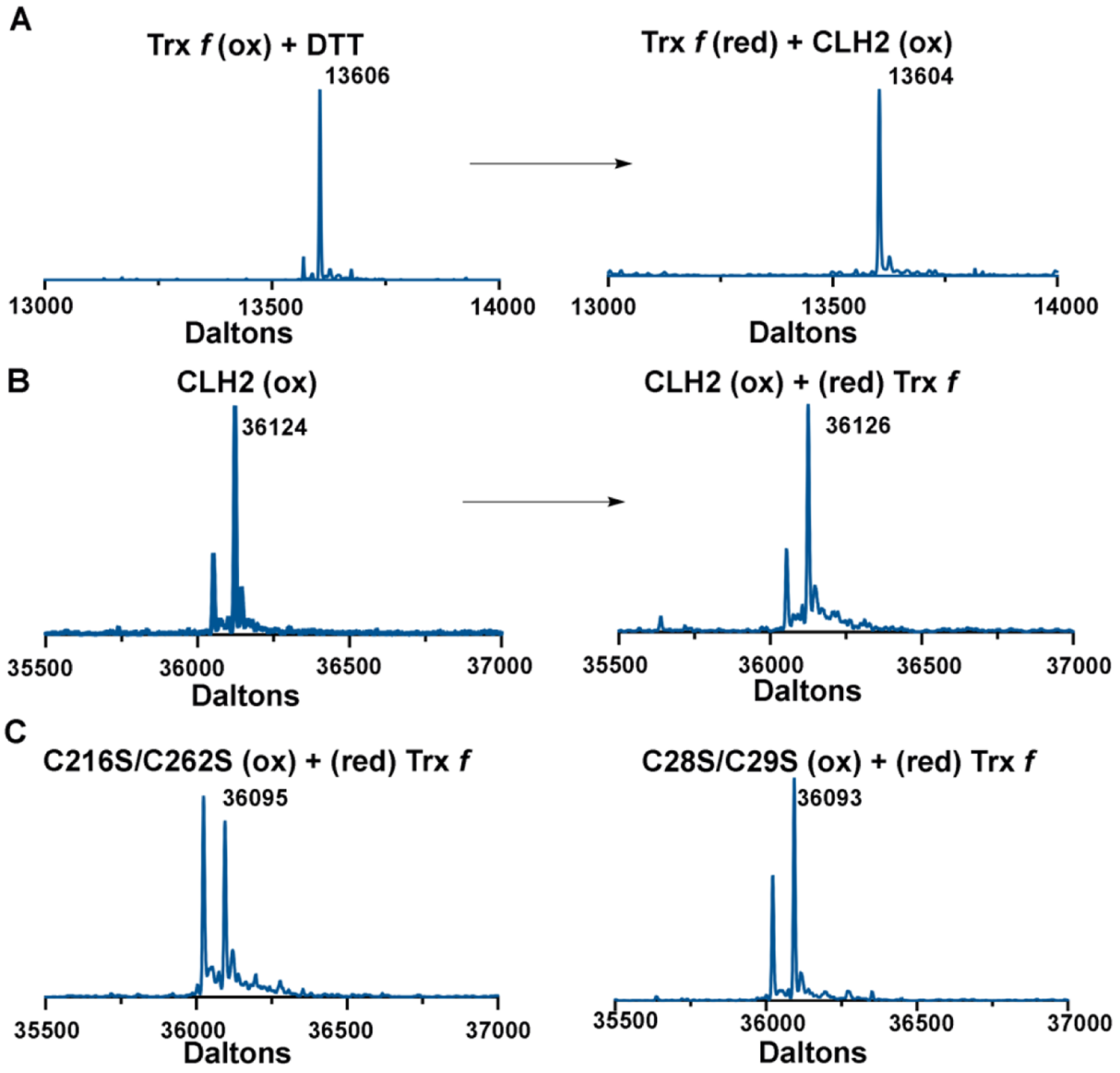

Figure 6. The N-terminal disulfide bond of *At*CLH2 can be reduced with a protein-based reductant. (A) As-purified Trx *f* exists with a single disulfide bond that can be reduced via anaerobic incubation with DTT (additional details are included in Figure S51). The Trx *f* disulfide bond can subsequently be reformed through incubation with *At*CLH2. (B) This incubation step also results in reduction of a single disulfide bond in *At*CLH2. (C) A H_2O_2-treated sample of the C216S/C262S variant (C216S/C262S (ox)) was desalted and incubated with a reduced and desalted sample of 30 μM Trx *f* ((red) Trx *f*). This experiment reveals that Trx *f* is competent to reduce the N-terminal disulfide bond of *At*CLH2. In contrast, the C28S/C29S variant which purifies with the active site disulfide bond intact, is not reduced by Trx *f*. For this panel, the expected masses of the double Cys-to-Ser variants is 36,095 Da.

measured activity of this variant is still higher than anticipated based on comparison to *Ta*chlorophyllase, an additional S135A/S138A variant was created and assessed with similar activity assays (Table 2 and, Figures 5C and S42). However, this variant shows similar activity and substrate preferences to the single variant.

The equivalent of the Phe residue in *Ta*chlorophyllase which constructs the oxyanion hole using its backbone atoms and forms part of the substrate binding site with its side chain was also probed.[14,32] In *At*CLH2, we determined that mutation of Tyr65 into its *Ta*chlorophyllase Phe counterpart results in creation of an *At*CLH2 protein that does not exhibit a clear preference for a Chl *a*, Chl *b*, or Phein *a* substrate in our assay (Table S4, Figures 5C, S40 and S43). The Y65F *At*CLH2 variant hydrolyzes each of these substrates to a similar extent, which is reminiscent of that observed with *Ta*chlorophyllase in an equivalent assay.[14] In terms of kinetic parameters, consistent with the altered substrate specificity of this *At*CLH2 variant, an approximate doubling in the Michaelis constant with a Chl *a* substrate is detectable for this protein. Combined with a distinct decrease in the k_{cat} of the hydrolysis reaction, the catalytic efficiency of this variant more closely resembles that of the Ser variants than the wild-type enzyme (Table 2 and Figure S43D).

Two additional *At*CLH2 variants were made to explore the importance of a second Tyr residue found at what appears, based on the AlphaFold[29,30] model of *At*CLH2, to occupy a position equivalent to the active site residue Phe72 in *Ta*chlorophyllase. This *T. aestivum* residue protrudes from the active site, is hypothesized to interact with the substrate, and corresponds to Tyr68 in *At*CLH2. Therefore, the activity profiles of *At*CLH2

https://doi.org/10.1021/acsbiomedchemau.4c00089
ACS Bio Med Chem Au 2024, 4, 353−370

Y68F and Y65F/Y68F variants were measured (Table S4 and Figures 5C and S44). From these variants, it was determined that the Y68F variant hydrolyzes Chl *a*, Chl *b*, and Phein *a* substrate pigments similarly to that observed with the wild-type enzyme (Table 2, Figures 5C and S44C−F). A Y65F/Y68F *At*CLH2 variant, on the other hand, appears to adopt a median level of activity relative to the two single variants. Most interestingly, this double variant exhibits the same trend in substrate selectivity as the wild-type enzyme, suggesting this second mutation at least partially compensates for the loss of selectivity noted in the Y65F single variant (Table 2, Figures 5C, and S44C−F). Finally, based on nearly equivalent T_m values for this set of *At*CLH2 variants, it appears that each of the noted changes in activity or substrate scope is directly correlated with a change in residue identity rather than an alteration in protein stability (Table 3 and Figure S45).

Disulfide Bonds of *At*CLH2 can be Reduced with Chemical and Protein-Based Reductants

As described above, the addition of DTT to *At*CLH2 results in reduction of two disulfide bonds, decreased catalytic activity, and reduced thermal stability (Tables 2, 3, Figures 4, S23, and S29B). To evaluate the extent of reductants that are similarly competent to affect *At*CLH2, intact mass spectrometry experiments were performed in the presence of tris(2-carboxyethyl)phosphine (TCEP), β-mercaptoethanol, and reduced glutathione (GSH). These experiments revealed that incubation of *At*CLH2 with either TCEP or β-mercaptoethanol results in partial reduction of the wild-type disulfide bond content, and similar, albeit less substantial decreases in T_m (ΔT_m of −1.5 to −3.9 °C, Table 3 and Figures S46A−C and S47). On the other hand, addition of an equivalent amount of GSH to *At*CLH2 results in a large mass increase (Figure S46D). This increase is consistent with the addition of one or multiple molecules of GSH to the protein, and again is representative of partial disulfide bond reduction (Figure S46D). Two similar experiments, which rely on incubation of GSH with the H_2O_2-treated C216S/C262S or C28S/C29S variants of *At*CLH2 also revealed the addition of either one or two molecules of GSH to the protein (Figure S48). As these variants, based on the data described above, presumably contain only the N-terminal or active site disulfide bond, respectively, this result suggests that both bonds are susceptible to reduction by GSH. For this reductant, and perhaps related to the observed GSH-mediated *S*-glutathionylation of *At*CLH2, a slight increase in the measured T_m is observed (Table 3 and Figure S47). As expected, all of the T_m data for *At*CLH2 in the presence of these small molecule reductants are in opposition to that measured with oxidants such as H_2O_2 or oxidized GSH (GSSG), which have only negligible impacts on the thermal stability of *At*CLH2 (Table 3 and Figure S47).

To further understand conditions that facilitate the reduction of *At*CLH2, a chloroplastic thioredoxin (Trx) protein, Trx *f*, from *A. thaliana* was recombinantly expressed and purified (Figures S49 and S50). Using intact mass spectrometry experiments, it was first identified that Trx *f* purifies in its oxidized form (Figure S51). Based on a sequence alignment of Trx *f* with *Spinacia oleracea* Trx *f*, this oxidized form likely contains a disulfide bond between two Cys residues from the characteristic Trp−Cys−Gly−Pro−Cys sequence motif (Figure S50).[33,34] As evidenced by a two-proton mass increase of the sample, anaerobic incubation of this oxidized sample with DTT results in reduction of this bond (Figure 6A). To test whether this DTT-treated and reduced sample of Trx *f* is competent to reduce *At*CLH2, DTT was desalted from the Trx *f* protein sample. This DTT-free, reduced sample of Trx *f* was subsequently incubated with as-purified *At*CLH2. Remarkably, this experiment resulted in formation of oxidized Trx *f* and a sample of *At*CLH2 that has one less disulfide bond than the as-purified wild-type enzyme (Figure 6A,B). This result indicates that Trx *f* can reduce a disulfide bond in *At*CLH2 (Figure 6B). However, unlike DTT, Trx *f* does not appear to have a significant impact on the hydrolysis activity of the enzyme (Figures 4 and S52).

To probe the identity of the disulfide bond being reductively cleaved by Trx *f*, an equivalent experiment was also performed with the H_2O_2-treated C216S/C262S variant, which contains just the N-terminal disulfide bond. As observed with the wild-type enzyme, Trx *f* is also capable of reducing this protein (Figure 6C). An analogous experiment with the C28S/C29S variant reveals that Trx *f*, however, is not competent to reduce the active site disulfide bond (Figure 6C). These results show that both disulfide bonds of *At*CLH2 are susceptible to reduction to small molecule reductants and only the N-terminal bond can be cleaved by Trx *f*.

DISCUSSION

Less than 1000 distinct protein folds have been suggested to exist in Nature.[35−38] This statement means that there are far less known accessible folds than there are encoded proteins. Therefore, to account for the vast and diverse set of enzymes used by living organisms, there must be mechanisms available to modulate, mix, or reprogram these existing core folds to exhibit attenuated activity or to facilitate a different type of chemistry.[38−40] Consistent with this notion, the α/β hydrolase enzyme superfamily encompasses a large set of proteins that use common catalytic machinery to function as esterases, lipases, peroxidases, dehalogenases, epoxide hydrolases, and proteases.[40−42] Quite interestingly, here, we show that even within just one functional class of this enzyme superfamily, two proteins can be tailored to exhibit markedly different biochemical properties. In principle, different catalytic efficiencies, substrate specificities, and reaction selectivities can be evolved in proteins by subtle changes or mutation of residues within the primary structure of a protein.[39] Similarly, changes to the quaternary structure can tune cooperativity, protein stability, and enzymatic activity.[39,43] Finally, gene duplication, gene fusion, and post-translational modification are each approaches that can be capitalized upon to further diversify the functions of a common protein scaffold.[39] For the chlorophyllases, the use of these protein tailoring strategies are exemplified: an inconsistent quaternary architecture, altered identities of primary sequence residues, a different pattern of Cys residues and number of disulfide bonds, relative to that observed in *Ta*chlorophyllase, support the creation of a protein that exhibits divergent catalytic properties. These alterations are likely in place to fine-tune *At*CLH2 to support the needs of *A. thaliana* and to cope with the environmental stressors and stimuli that are native to the environmental niches that *A. thaliana* inhabits. Alternatively, and as previously suggested, it is possible that the protein is instead tailored to the characteristic "ROS signature" of the compartment that it inhabits.[7] Regardless of the reason, for all photosynthetic organisms, these coping mechanisms are imperative to maintain steady state levels of Chl, prevent photodamage, and to support the process of photosynthesis.[3,4]

https://doi.org/10.1021/acsbiomedchemau.4c00089
ACS Bio Med Chem Au 2024, 4, 353−370

First and foremost, in this work, it is shown that *At*CLH2 behaves as a monomer in solution (Figure 2). Because *Ta*chlorophyllase, which shares 47% sequence identity with *At*CLH2 exists as a dimeric species in crystallo[14] as well as in similar solution-based conditions (Figures 1, 2, and S3), this finding was unexpected. However, based on the suggestion that proteins, which share on the order of 30−40% sequence identity, are only about 70% likely to showcase the same oligomeric state,[44] and the several known examples of α/β hydrolases that function as monomers, dimers, or higher-order oligomers,[41] this switch in oligomeric state is certainly not unprecedented. In fact, in cases where homooligomerization is not used to support cooperativity, such as in the Chl dephytylase enzyme class,[14] it is possible that more variation in quaternary structure should be expected. As far as the reason for the observed differences between *Ta*chlorophyllase and *At*CLH2, some studies suggest higher order oligomeric states lend to enhanced protein thermal stabilities.[39,45,46] Consistent with this idea, here it is identified that the T_m of *At*CLH2 is 59.4 ± 0.3 °C (Table 3 and Figure S29), an approximate 25 °C less than that previously measured for *Ta*chlorophyllase (74.8 ± 0.8 °C[14]). Furthermore, in support of the proposal that higher order assemblies endow greater stability to a protein, rational mutations designed to disrupt the dimeric *Ta*chlorophyllase structure, are also shown, in this work, to influence thermal stability (Table 3 and Figure S30). Alternatively, as our previous work indicates that dimeric *Ta*chlorophyllase contains five disulfide bonds,[14] it is also possible that the lack of equivalent number of covalent linkages in *At*CLH2 is, at least partially, responsible for the measured differences in T_m (Figure S4). In fact, a range of native and engineered α/β hydrolases have been shown to embody elevated stabilities in the presence of these bonds.[47−49] Building on studies which have indicated that both post-translational modification and the binding of a small molecule at an interface can favor oligomerization,[46] it was also investigated whether the absence of the divalent metal ion coordinating and weak interaction forming residues found at the *Ta*chlorophyllase dimeric interface are the culprit of the monomeric nature of *At*CLH2. Indeed, here it is shown that changes in the identity of these residues in *Ta*chlorophyllase, as described above, do appear to have an effect on T_m and correspondingly are anticipated to contribute to the stability of the dimeric structure (Table 3 and Figure S30). However, as comparison of the *Ta*chlorophyllase and *At*CLH2 primary sequences and available models for these enzymes is insufficient to rationally alter the oligomeric states of these enzymes, future *At*CLH2 structural studies are needed to understand the molecular basis for the architectural differences.

Here, the *At*CLH2 protein scaffold is further demonstrated to support a lower level of hydrolysis activity on Chl*a* in vitro relative to *Ta*chlorophyllase.[14] Yet, despite the differences in the measured kinetic parameters of wild-type *At*CLH2 and *Ta*chlorophyllase, several parallels between the activity of these enzymes can still be drawn. For example, both proteins show a preference for hydrolyzing Chl *a* relative to other available pigment substrates (Table 2 and Figure 5A). Disruption of the disulfide bond formed between the equivalent of Cys residues at the 216 and 264 positions has the largest overall impact on enzyme activity in both homologues (Table 2, Figures 4, S22 and S24). *At*CLH2 Cys-to-Ser variants at these positions showcase both decreased k_{cat} and K_M values (Table 2). As previously described, the typical α/β hydrolase mechanistic proposal proceeds via covalent catalysis, meaning that whereas k_{cat} informs on the dismantling of the covalent acyl-enzyme intermediate, K_M reports on the kinetics involved in forming the enzyme−substrate complex.[14] Therefore, as described for *Ta*chlorophyllase, disruption of the active site disulfide bond perhaps allows Chl *a* to more easily react with the active site Ser nucleophile. Release of the hydrolysis product, however, must in some way, be compromised.[14]

Impairment of product release in some of the tested *At*CLH2 variants may be attributable to not only loss of the active site disulfide bond, but also disruption of what has been coined the "catalytic acid zone".[41] This zone involves a series of residues that use hydrogen bonds to ensure that the catalytic His residue is maintained in a proper orientation for catalysis.[41] We hypothesize that for *At*CLH2, consistent with that observed for *Ta*chlorophyllase,[14] disruption of the active site disulfide bond, which like a seatbelt, links one Cys residue on the His-containing loop to a second Cys residue located within the core of the α/β hydrolase fold, should certainly impact the positioning of catalytic triad residues (Figure 7). In this scenario, product release, which relies on the catalytic triad His-residue, would be impaired and thereby provides an explanation for the observed negative impacts on the k_{cat} of the C216S, C264S, C216S/C264S, and C216S/C262S protein variants (Table 2, Figures 7, and S24). Likewise, it is intuited that the increased flexibility of these variants imparted by the loss of the active site disulfide linkage, account for the nominal

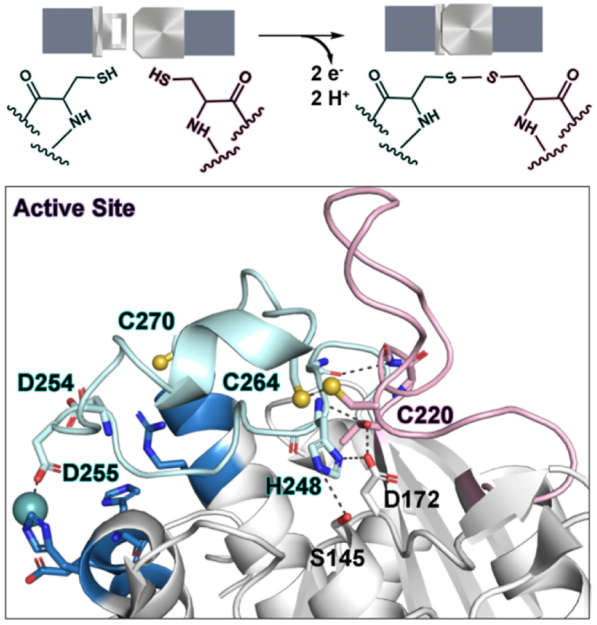

Figure 7. The active site disulfide bond of *Ta*chlorophyllase acts like a seatbelt to maintain the proper orientation of residues in the catalytic acid zone. Opening of the seatbelt likely leads to disorder, which inhibits the optimal positioning of the catalytic triad residues (Ser145, His248, and Asp172). Disorder among the catalytic triad residues should negatively impact catalysis. The His loop (cyan) in *Ta*chlorophyllase (PDB: 8FJD[14]) appears to be held in place by the buckle (Cys220) and latch (Cys264) of the seatbelt, and by the belt attached to the latch, which involves the dimeric interface residues that coordinate a metal ion or form electrostatic interactions with the adjacent protomer of the enzyme. As described in this work, the lack of a dimeric architecture, divalent metal ion binding site, and intermolecular disulfide bond, likely means that the catalytic acid zone of *At*CLH2 exhibits more flexibility.

https://doi.org/10.1021/acsbiomedchemau.4c00089
ACS Bio Med Chem Au 2024, 4, 353−370

level of hydrolysis that is observed with the non-rigid Phein *a* molecule, relative to the planar Chl *a* and *b* substrates. A similar explanation can also be used to comprehend the observed alterations in the kinetic parameters of the S138A and Y65F variants, which not only change the identity of key catalytic residues, but would also be expected to perturb the arrangement of residues located within the catalytic acid zone. The *At*CLH2 C230S variant also has low activity. In fact, the kinetic parameters of the C230S variant resemble those of the active site disulfide bond variants (Table 2). In *Ta*chlorophyllase, the equivalent of Cys230 is Cys234, which forms a disulfide bond with Cys238. These residues are found in the secondary structure elements that connect Cys220 to the catalytic triad His-residue (Figure S4). Again, changes of the side chain properties in this location may also propagate to perturb the positioning of the residues in the catalytic acid zone. In *Ta*chlorophyllase, dimeric interface residues such as those that are used to coordinate the divalent metal ion (His76 and Asp255), or to form covalent (Cys270), and electrostatic (Glu79, His80, and Asp254) interactions at the interface are also found on the His-containing loop (Figure 7). In line with our assertions regarding alterations to the catalytic acid zone and impaired hydrolysis activity, triple, quintuple, and sextuple dimeric interface variants of *Ta*chlorophyllase each exhibit decreased k_{cat} values (Table 2 and Figure S25). Likewise, and akin to a recent report, it is also plausible that *Ta*chlorophyllase dimerization may propagate dynamic motions that support high levels of chlorophyllase-mediated Chl *a* hydrolysis activity.[50−52] Additional investigation into how this latter option affects catalysis is paramount. However, at this point, we posit that the lack of the *Ta*chlorophyllase dimeric interface interactions (including the Cys270 disulfide bond), and the lack of the Cys234−Cys238 disulfide bond likely result in disordering of the catalytic acid zone, or flexibility of the His loop, and the positions of the catalytic triad residues. These disruptions then account for the approximate 7-fold decrease in the measured k_{cat} of *At*CLH2 relative to *Ta*chlorophyllase (Table 2 and Figure 7).

Finally, here, it is shown that the disulfide bonds of *At*CLH2 can be reduced by small molecule reductants. DTT, TCEP, β-mercaptoethanol, and GSH each impact the as-purified structure of *At*CLH2. Whereas DTT can reduce both the N-terminal and active site disulfide bonds, the other reductants only afford partial reduction. For these molecules, incomplete disulfide bond reduction in vitro is not unexpected. Both GSH (−0.26 V) and β-mercaptoethanol (−0.26 V) have higher reduction potentials than DTT (−0.33 V).[53,54] TCEP, on the other hand, which is generally considered to have a more negative potential than DTT, may be unable to easily access the formed *At*CLH2 disulfide bonds due to its larger chemical structure.[54,55] Again, this result contrasts what is observed with *Ta*chlorophyllase for which an excess amount of DTT, TCEP, or GSH have no impact on the disulfide bond character or in vitro activity of the protein.[14] Based on the structure of *Ta*chlorophyllase, it certainly appears plausible that a small molecule cellular reductant, but not a protein-based reductant, could access the active site disulfide bond (Figure S53). However, this disulfide bond is not reduced by these small molecules in vitro.[14] Therefore, we hypothesize that the purported decreased flexibility of the dimeric *Ta*chlorophyllase protein scaffold, relative to the monomeric *At*CLH2 architecture, is the reason for the observed differences. At this point additional studies are needed to identify whether the chlorophyllase homologue active site disulfide bonds can undergo cycles of oxidation and reduction, and how these changes in Cys residue oxidation state are facilitated in vivo.

It is also demonstrated in this work that the N-terminal disulfide bond of *At*CLH2 can be cleaved by Trx *f*. This bond, which is formed between two sequence-adjacent Cys residues, is a rare find in a protein due its strained geometric arrangement.[56] Nevertheless, a similar disulfide bond, has previously been identified in the cyanobacterial transcription factor RexT.[37] This protein functions as a sensor of H_2O_2, and in its oxidized, vicinal disulfide bond-containing state, allows for increased expression of a thioredoxin protein known as TrxA2.[37] Akin to what we observe with *At*CLH2, in RexT, the sequence adjacent Cys-residue formed disulfide bond is also reduced by a thioredoxin protein, although here, the implicated thioredoxin protein is TrxA2.[57] This latter point coupled with our observation that disruption of the N-terminal disulfide bond has a less significant impact on the catalytic activity of *At*CLH2, relative to the active site disulfide bond, suggests that this bond could serve an alternative type of regulatory role in *At*CLH2. One possibility is that the oxidation state of this bond, as observed in RexT,[37] is involved in a structural change that regulates the ability of this enzyme to interact with a partner biomolecule in the cell. However, at this point, further investigation is needed to clarify the role of this N-terminal linkage and to identify the native reductants for this N-terminal disulfide bond of *At*CLH2 in vivo.

The ability of both small molecule and protein-based reductants to reduce the disulfide bonds in *At*CLH2, and affect a catalytic response, highlights an important link with other Chl metabolic proteins such as Mg^{2+}-chelatase, Mg^{2+}-protoporphyrin IX methyltransferase, and NON-YELLOWING/STAY GREEN1.[58,59] These proteins, which are also proposed to be controlled via the oxidation state of Cys residues, are thought to synchronize the biosynthesis and degradation of Chl pigments with environmental conditions.[58−62] We hypothesize that more broadly, for chlorophyllases, the well-conserved active site disulfide bond forming Cys residues[14] and others found in the primary sequence are used to respond to unpredictable environmental stressors. More specifically, they function as precisely tuned redox switches to adapt the α/β hydrolase protein architecture to catalyze its reaction in alignment with the evolving needs of an organism. Last, we posit that the identities of the residues found at the dimeric interface of *Ta*chlorophyllase warrant further investigation in other homologues as they too appear to function as dials that have the ability to custom tune the hydrolysis activity of chlorophyllase. Studies into the diversity of sequence−structure−function relationships throughout the protein family are ongoing to illuminate the regulatory mechanisms that photosynthetic organisms use to degrade Chl pigments in different environmental niches.

EXPERIMENTAL PROCEDURES

Purification of *At*CLH2

A construct of C-terminally His-tagged CLH2 (Uniprot: Q9M7I7) was codon-optimized for *E. coli* expression, synthesized, and cloned into a pET21(d+) vector by Genscript. This construct was transformed into *E. coli* C41 (DE3) cells. In all purifications, a 10 mL overnight culture was used to inoculate 1 L of Lysogeny Broth−Miller formulation (LB) media supplemented with ampicillin (50 mg/L). The cultures were then grown at 37 °C until the OD_{600} measured 1.0. A subsequent induction with 0.5 mM isopropyl β-D-1-thiogalactopyranoside (IPTG) and overnight incubation at 17 °C allowed for recombinant production of *At*CLH2. Following a centrifugation step, the *At*CLH2-containing *E. coli* cells were resuspended in a lysis buffer containing 20 mM

https://doi.org/10.1021/acsbiomedchemau.4c00089
ACS Bio Med Chem Au 2024, 4, 353−370

tris(hydroxymethyl)aminomethane hydrochloride (Tris-HCl, pH 7.5), 150 mM NaCl, 5 mM imidazole and 5% (v/v) glycerol. After cellular resuspension, a 10 min program that involved a cycling of steps (5 s of sonication with 10 s rest) at 30% amplitude was used for cell lysis. The supernatant from the sonication step was loaded onto a 5 mL Ni-NTA column (Cytiva) which was pre-equilibrated with the above-defined lysis buffer. After loading the supernatant on the column, two wash steps were performed: first a 12-column volume wash step was run with lysis buffer and second, a 6 column volume wash step was run with a buffer that contained 20 mM Tris-HCl (pH 7.5), 150 mM NaCl, 50 mM imidazole, and 5% (v/v) glycerol. Finally, the protein was eluted from the column using a buffer that consisted of 20 mM Tris-HCl (pH 7.5), 150 mM NaCl, 200 mM imidazole, and 5% (v/v) glycerol. Purified *At*CLH2 was concentrated and loaded on a Superdex 200 size exclusion column which was pre-equilibrated in buffer containing 50 mM 4-(2-hydroxyethyl)-1-piperazine-ethanesulfonic acid (HEPES, pH 7.5), 150 mM NaCl, and 5% (v/v) glycerol. As described above, *At*CLH2 eluted from this column at a retention time that would be consistent with it behaving as a monomeric species in solution. This conclusion is made based off of comparison to a commercially purchased protein standard that was run on the same column (Bio-Rad).

Purification of Wild-Type and *Ta*chlorophyllase Variant Proteins

The methods for expressing and purifying *Ta*chlorophyllase and its variants were previously described and followed here.[14] In brief, cell pellets were resuspended in 50 mM Tris-HCl (pH 8.0), 150 mM NaCl, 20 mM imidazole, and 5% (v/v) glycerol. Following completion of the sonication cycle described above, the supernatant was loaded onto a 5 mL Ni-NTA column and *Ta*chlorophyllase was eluted with 50 mM Tris-HCl (pH 8.0), 150 mM NaCl, 300 mM imidazole, and 5% (v/v) glycerol. The protein was then concentrated and loaded onto a Superdex 200 size exclusion column pre-equilibrated with 50 mM HEPES (pH 8.0), 150 mM NaCl, and 5% (v/v) glycerol. Fractions containing purified *Ta*chlorophyllase were concentrated and flash frozen for storage at −80 °C.

Purification of *A. thaliana* Trx *f*

The gene encoding Trx *f* (Uniprot: Q9XFH8) minus the first 57 residues was synthesized, codon optimized, and cloned into a pMCSG-9 vector by Genscript. The N-terminal region was truncated due to its prediction as a chloroplastic targeting sequence using the TargetP 2.0 Database.[63] This construct was transformed into *E. coli* BL21 (DE3) cells and grown in a 5 mL overnight starter culture, which was used to inoculate 1 L flasks of LB media containing 50 mg/L ampicillin. These 1 L cultures were then incubated at 37 °C until the OD_{600} approached 0.7. At this point, protein expression was induced with 0.5 mM IPTG and the cultures were subsequently incubated and shaken at 16 °C overnight. Cells were resuspended in 20 mM Tris-HCl (pH 7.5), 150 mM NaCl, and 5% (v/v) glycerol, sonicated, and centrifuged as described above. The supernatant was loaded onto a 5 mL MBPTrap column (Cytiva) using the same sonication buffer and eluted with 20 mM Tris-HCl (pH 7.5), 150 mM NaCl, 10 mM maltose, and 5% (v/v) glycerol. Elution fractions were then pooled and dialyzed into 1 L of buffer containing 50 mM HEPES (pH 7.5) and 150 mM NaCl for tag cleavage with *Tobacco Etch Virus* protease. The dialyzed sample was then loaded onto a Ni-NTA column (Cytiva) and diluted with a buffer containing 50 mM Tris-HCl (pH 7.5), 150 mM NaCl, and 20 mM imidazole. Fractions containing the cleaved Trx *f* were buffer exchanged into storage buffer containing 50 mM HEPES (pH 7.5), 150 mM NaCl, and 5% (v/v) glycerol before being concentrated and flash frozen for storage −80 °C.

Production of *At*CLH2 Variants

To investigate the impact of changing the identity of the amino acid residues in *At*CLH2 on the activity and stability of the protein, variants were created using either the QuikChange Lightning Site-Directed Mutagenesis Kit (Agilent) or the Q5 Site-Directed Mutagenesis Kit (NEB). The primers used in this work were purchased from Integrated DNA Technologies (Supporting Information Table 1). Incorporation of the desired mutations into the *At*CLH2 plasmid was evaluated using sanger DNA sequencing (Genewiz). All confirmed variant plasmids were transformed into *E. coli* C41 (DE3) cells and purified using the method described for wild-type *At*CLH2 above.

Preparation of Pigments

The chlorophyll (Chl) *a*, Chl *b*, and bacteriochlorophyll (BChl) *a* pigments used in this work were purchased from Sigma-Aldrich or Frontier Scientific. In contrast, the 7-hydroxymethyl Chl *a* pigment used in this work was produced via the reduction of Chl *b* and previously described methods.[64] More specifically, to create this pigment, 3 mL of methanol and 1 mg of $NaBH_4$ were added to a 1 mM stock of Chl *b*. This step created 7-hydroxymethyl Chl *a* and was followed by a quench with aqueous NaCl, and solvent evaporation. All Chl substrates were prepared in DMSO to a final concentration of 10 mM for activity experiments. For the kinetic experiments described below, 1 mM stock concentrations of the pigments were prepared in acetone to support the needed liquid−liquid phase extraction step. The solvents used to prepare the pigment stocks mirror those used in previous work.[14,64]

Kinetic Experiments

The Michaelis−Menten kinetic parameters were measured using *Ta*chlorophyllase, *Ta*chlorophyllase variants, His-tagged *At*CLH2, or His-tagged *At*CLH2 variants. These values were calculated using a colorimetric assay and previously developed protocols.[14,31] Specifically, all reactions performed here were made to contain protein, different concentrations of Chl *a*, 50 mM HEPES (pH 7.5), 150 mM NaCl and 5% (v/v) glycerol. For these reactions, the concentration of Chl *a* was varied between 5 and 450 μM (*Ta*chlorophyllase) or 10 to 400 μM (*At*CLH2). To ensure that the reactions were conducted under Michaelis-Menten conditions, either previously identified conditions (*Ta*chlorophyllase,[14]), or a range of protein concentrations (10−100 nM) for wild-type *At*CLH2 and the variants were used. More specifically, a protein concentration of 100 nM was used for the C216S and C230S *At*CLH2 variants. For the C262S variant, an enzyme concentration of 10 nM was used. For all other variants and the wild-type *At*CLH2 protein, an enzyme concentration of 50 nM was used. All reactions had a final volume of 300 μL, and all reactions were initiated by the addition of substrate, incubated for 2 min at 25 °C, and were quenched with 150 μL of a solution that contained acetone, hexane, and 10 mM NaOH in a 4:6:1 ratio. Following the quench step, all reactions were centrifuged at 12,000*g* for 10 min and a liquid−liquid extraction was used to liberate the Chlide *a* product from the reaction mixture. The concentration of product formed was measured using an Epoch 2 microplate spectrophotometer (BioTek) and was calculated using the absorbance at 665 nm and an extinction coefficient of 54.1 mM^{-1} cm^{-1}.[65] For wild-type *At*CLH2, the kinetic parameters were also measured with a Chl *b*, pheophytin *a*, and Bchl *a* substrate. For these substrates, extinction coefficients of 42.0 mM^{-1} cm^{-1} at 650 nm, 47.2 mM^{-1} cm^{-1} at 667 nm and 42.1 mM^{-1} cm^{-1} at 773 nm were used to calculate the amount of product formed, respectively.[65,66] The kinetic values were determined using GraphPad Prism software. All reaction measurements were performed in triplicate.

Activity Experiments

All of the activity measurements (represented in bar graphs) for this work were performed using His-tagged versions of *At*CLH2 and its variants. The methods were designed to mirror those previously described with small deviations.[14] Each reaction was first analyzed to determine the amount of Chl *a* substrate needed to saturate the enzyme. For this endeavor, 150 μL reactions were prepared that contained 5 μM *At*CLH2, 0.1−1 mM Chl *a*, and 50 mM Tris-HCl (pH 7.5). Following a 35 min dark incubation at 30 °C, these samples were quenched with 300 μL of a solution composed of acetonitrile and 0.5 mM of an internal standard (acetaminophen). A centrifugation step at 17,000*g* for 10 min was performed before triplicate samples were analyzed using a Thermo Scientific UltiMate 3000 HPLC with an Agilent ZORBAX SB-AQ 5 μm 4.6 × 150 mm column. The method used for pigment analysis required injection of a 40 μL sample and two solvents (solvent A: 85:15 methanol: 50 mM ammonium acetate (pH 5.2) and solvent B: methanol). A 15 min isocratic flow of solvent A

https://doi.org/10.1021/acsbiomedchemau.4c00089
ACS Bio Med Chem Au 2024, 4, 353−370

followed by an additional 15 min isocratic flow of solvent B were employed for used for separation of Chl *a* from the product, Chlide *a*. This first analysis revealed that activity of *At*CLH2 reached a maximum at concentrations above 0.5 mM Chl *a*.

To calculate the activity of the different *At*CLH2-containing reactions, different concentrations of substrates and/or products were used to create standard curves. To accomplish this task, 150 μL samples that contained varying concentrations of Chl *a*, Chl *b*, Bchl *a*, Phein *a*, or 7-hydroxymethyl Chl *a* in 20 mM Tris-HCl (pH 7.5), were prepared. These samples were incubated at 30 °C for 1 h in the dark and were quenched with 300 μL of acetonitrile containing an internal standard (acetaminophen). For the separation of Chlide *a* from Chl *a*, the HPLC method described above was implemented. For the separation of Chl *b*, Bchl *a*, Phein *a*, and 7-OH Chl *a* from their respective products, a different method was employed. This method also used the ZORBAX SB-AQ 5 μm 4.6 × 150 mm column but instead consisted of a 15 min isocratic flow of solvent C (a solution of acetonitrile/methanol/ethyl acetate in a 60:20:20 ratio). For all pigments, the identity of the substrate and product peaks was confirmed using electrospray ionization (ESI)-MS and an Agilent 6230 time-of-flight (TOF) mass spectrometer.

The plotted activity values for *At*CLH2 and its variants were calculated from triplicate 150 μL reactions. For wild-type *At*CLH2, the activity values with various substrates were calculated from 150 μL reactions containing 2 μM protein, 250 μM substrate, and 20 mM Tris-HCl (pH 7.5) that were quenched and injected onto the HPLC as described above. The *At*CLH2 variant activity values, on the other hand, were assembled to contain 5 μM protein, 500 μM substrate, and 20 mM Tris-HCl (pH 7.5). All reactions were allowed to progress at 30 °C for 35 min before a quench with 300 μL of acetonitrile containing an acetaminophen internal standard. Substrate consumption was used to quantitatively measure the activity for the a Chl *a*, Chl *b*, Bchl *a*, and 7-hydroxymethyl Chl *a* reactions, as none of these substrates have commercially available product standards. Pheophorbide *a* is the commercially available product of Phein *a*, and therefore for the hydrolysis of Phein *a*, product formation was used to measure activity. The activity was calculated using the following equation: (the amount of substrate consumed)/(the final concentration of *At*CLH2, 5 μM). Because the activity with a Chl *a* substrate is monitored by integration of the amount of substrate remaining at the end of the experiment, these calculations approached the limit of detection on our instrument (meaning that a lot of substrate was consumed).

SEC and Light Scattering Experiments

Samples of *At*CLH2 and *Ta*chlorophyllase were thawed on ice, centrifuged at 4 °C and 14,000*g* for 10 min and separated by size at 25 °C on an Agilent 1260 Infinity II HPLC system using a Yarra 3 μm SEC-2000 300 × 7.8 mm size-exclusion column (Phenomex). Injections of 15 μL were used for each run. For *At*CLH2, the mobile phase was 50 mM HEPES pH 7.5, 200 mM NaCl, and 5% (v/v) glycerol. For *Ta*chlorophyllase, the mobile phase was 50 mM HEPES pH 7.5, 150 mM NaCl, and 5% (v/v) glycerol. A 0.4 mL/min flow rate was used. Eluent from the size-exclusion column was monitored using a DAWN MALS instrument (Wyatt) and an Optilab differential refractive index instrument (Wyatt). A NanoStar II DLS instrument (Wyatt) was used with a 2 μL quartz cuvette (Wyatt) to collect three 5 s acquisitions separated by 1 min. For the H76S/E79S/H80Q/R83L/C270S and H76S/E79S/H80Q/R83L/C270S/G272R variants, DLS data were collected using Wyatt disposable microcuvettes with ten averaged acquisitions. Instrument performance was monitored using injections of a bovine serum albumin standard. SEC-MALS data were analyzed using Astra Software version 8.2 and DLS data were analyzed using Dynamics Software version 8.2.

Differential Scanning Fluorimetry

To measure the melting temperatures (T_m) of the wild-type *At*CLH2, *At*CLH2 variants, and *Ta*chlorophyllase variants, a QuantStudio 3 Real-Time PCR system (Thermo Fisher Scientific) was used according to previously described methods.[14] In short, 15 μM of protein in buffer (50 mM HEPES (pH 7.5), 150 mM NaCl, and 5% (v/v) glycerol) was mixed with an 8-fold dilution of SYPRO Orange dye (Applied Biosystems). All T_m values were measured in quadruplicate and were calculated from experiments that employed a method of heating from 25 to 99 °C at a rate of 0.05 °C per second. The SYPRO Orange dye fluorescence signal was recorded at a wavelength of 570 nm. Melting temperatures were calculated from derivative fluorescence curves and analyzed using Applied Biosystems Protein Thermal Shift Software v1.4 (Thermo Fisher Scientific).

Intact Protein Mass Spectrometry

To understand the state of the *At*CLH2 Cys residues in as-purified *At*CLH2 and its variants, intact mass spectrometry experiments were performed. These experiments generally followed methods that were previously described.[14] For this work, *At*CLH2 and its Cys-to-Ser variants were diluted to a concentration of 10 μM in 20 mM Tris-HCl (pH 7.5) and assessed using an Agilent G6545A quadrupole-TOF mass spectrometer equipped with a dual AJS ESI source. All LC−MS experiments were conducted using an Aeris WIDEPORE C4 column (2.1 × 50 mm, 3.6 μm, 200 Å) (Phenomenex). All results were analyzed in the Agilent MassHunter Bioconfirm software.

Samples (20 μL) that were alkylated were incubated at 30 °C for 45 min in the presence of 10 mM IAA. Samples (20 μL) that were reduced with DTT were incubated at 30 °C for 30 min in the presence of 10 mM DTT. Last, for samples that were reduced and subsequently oxidized, the sample (20 μL) was incubated with 10 mM DTT for 30 min, desalted via a Bio-Spin P-6 column (Bio-Rad), and incubated with 20 μL of 400 μM H_2O_2 (final concentration in the sample is 200 μM H_2O_2). To identify the state of the Trx *f* Cys residues, 50 μL of Trx *f* was incubated with 10 mM DTT on cold beads in a Coy anaerobic chamber for 45 min and subsequently desalted with a Bio-Spin P-6 column (Bio-Rad). Experiments conducted to observe the effect of incubating Trx *f* with *At*CLH2 were performed anaerobically. In brief, 10 μM *At*CLH2 or its variants were combined with 20 μM Trx *f* in 20 mM Tris-HCl (pH 7.5) for 30 min at room temperature in an anaerobic chamber.

Bioinformatics

The chlorophyllase sequence similarity network, shown in Figure 1 was visualized using Cytoscape 3.8.2[67] and created using the EFI-EST and previously described methods.[14] In short, an SSN was generated from the chlorophyllase (IPR017395) protein family that consists of 1832 chlorophyllases that are represented as individual nodes.

■ ASSOCIATED CONTENT

Data Availability Statement

This article contains Supporting Information.

Supporting Information

The Supporting Information is available free of charge at https://pubs.acs.org/doi/10.1021/acsbiomedchemau.4c00089.

This article contains supporting information, which is composed of 7 tables and 53 figures that contain the underlying data for figures in the main text as well as additional experimental results referred to in the main text document (PDF)

■ AUTHOR INFORMATION

Corresponding Author

Jennifer Bridwell-Rabb − *Department of Chemistry, University of Michigan, Ann Arbor, Michigan 48109, United States;* orcid.org/0000-0002-7437-6217; Email: jebridwe@umich.edu

Authors

Madison Knapp − *Department of Chemistry, University of Michigan, Ann Arbor, Michigan 48109, United States;* orcid.org/0000-0002-5392-2282

https://doi.org/10.1021/acsbiomedchemau.4c00089
ACS Bio Med Chem Au 2024, 4, 353−370

Minshik Jo − *Department of Chemistry, University of Michigan, Ann Arbor, Michigan 48109, United States*
Courtney L. Henthorn − *Department of Chemistry, University of Michigan, Ann Arbor, Michigan 48109, United States*
Marley Brimberry − *Department of Chemistry, University of Michigan, Ann Arbor, Michigan 48109, United States*
Andrew D. Gnann − *Department of Chemistry, University of Massachusetts Boston, Boston, Massachusetts 02125, United States*
Daniel P. Dowling − *Department of Chemistry, University of Massachusetts Boston, Boston, Massachusetts 02125, United States*

Complete contact information is available at:
https://pubs.acs.org/10.1021/acsbiomedchemau.4c00089

Author Contributions

M.K., M.J., C.L.H., M.A.B., and J.B.R. contributed to the design of the experiments and wrote the manuscript. M.J. and M.K. produced all proteins and variants used in this work, performed the activity assays, and obtained all HPLC and MS data. M.J., M.K., and C.L.H. performed thermal shift experiments. D.P.D. and A.D.G. performed the DLS and SEC-MALS experiments. CRediT: **Madison Knapp** conceptualization, data curation, formal analysis, investigation, methodology, validation, visualization, writing - original draft, writing - review & editing; **Minshik Jo** conceptualization, data curation, formal analysis, investigation, methodology, validation, visualization, writing - original draft, writing - review & editing; **Courtney L Henthorn** data curation, investigation, methodology, validation, visualization, writing - original draft, writing - review & editing; **Marley A Brimberry** data curation, investigation, methodology, visualization, writing - original draft, writing - review & editing; **Andrew D Gnann** data curation, formal analysis, investigation, methodology, validation, writing - review & editing; **Daniel P. Dowling** data curation, formal analysis, investigation, methodology, validation, writing - review & editing; **Jennifer Bridwell-Rabb** conceptualization, formal analysis, funding acquisition, investigation, methodology, project administration, supervision, validation, visualization, writing - original draft, writing - review & editing.

Funding

This material is based upon work supported by the was supported by the U.S. Department of Energy, Office of Science, Office of Basic Energy Sciences, under Award Number DE-SC0021240 (J.B.R.) and the Beckman Young Investigator Program (J.B.R.).

Notes

The authors declare no competing financial interest.

■ ACKNOWLEDGMENTS

The authors acknowledge helpful discussions with David Boggs and Alejandro Arcadio Garcia as well as the Biophysical Instrumentation Core at the University of Massachusetts Boston, funded by the Massachusetts Life Sciences Center.

■ REFERENCES

(1) Knapp, M.; Bridwell-Rabb, J. The green pigment of life. *Nat. Chem.* **2022**, *14*, 1202.
(2) Hendry, G. A. F.; Houghton, J. D.; Brown, S. B. The Degradation of Chlorophyll - a Biological Enigma. *New Phytol.* **1987**, *107*, 255−302.
(3) Lin, Y. P.; Charng, Y. Y. Chlorophyll dephytylation in chlorophyll metabolism: a simple reaction catalyzed by various enzymes. *Plant Sci.* **2021**, *302*, 110682.
(4) Tanaka, A.; Tanaka, R. Chlorophyll metabolism. *Curr. Opin. Plant Biol.* **2006**, *9*, 248−255.
(5) Imlay, J. A. Pathways of oxidative damage. *Annu. Rev. Microbiol.* **2003**, *57*, 395−418.
(6) Latifi, A.; Ruiz, M.; Zhang, C. C. Oxidative stress in cyanobacteria. *FEMS Microbiol. Rev.* **2009**, *33*, 258−278.
(7) Choudhury, F. K.; Rivero, R. M.; Blumwald, E.; Mittler, R. Reactive oxygen species, abiotic stress and stress combination. *Plant J.* **2017**, *90*, 856−867.
(8) Dumanovic, J.; Nepovimova, E.; Natic, M.; Kuca, K.; Jacevic, V. The Significance of Reactive Oxygen Species and Antioxidant Defense System in Plants: A Concise Overview. *Front. Plant Sci.* **2021**, *11*, 552969.
(9) Yu, B. P. Cellular defenses against damage from reactive oxygen species. *Physiol. Rev.* **1994**, *74*, 139−162.
(10) Lee, S.; Kim, S. M.; Lee, R. T. Thioredoxin and thioredoxin target proteins: from molecular mechanisms to functional significance. *Antioxid. Redox Signaling* **2013**, *18*, 1165−1207.
(11) Willstaetter, R.; Stoll, A. Examinations on chloropyll. XI Chlorophyllase. *Justus Liebigs Ann. Chem.* **1911**, *378*, 18−72.
(12) Schenk, N.; Schelbert, S.; Kanwischer, M.; Goldschmidt, E. E.; Dormann, P.; Hortensteiner, S. The chlorophyllases AtCLH1 and AtCLH2 are not essential for senescence-related chlorophyll breakdown in Arabidopsis thaliana. *FEBS Lett.* **2007**, *581*, 5517−5525.
(13) Hu, X.; Jia, T.; Hortensteiner, S.; Tanaka, A.; Tanaka, R. Subcellular localization of chlorophyllase2 reveals it is not involved in chlorophyll degradation during senescence in Arabidopsis thaliana. *Plant Sci.* **2020**, *290*, 110314.
(14) Jo, M.; Knapp, M.; Boggs, D. G.; Brimberry, M.; Donnan, P. H.; Bridwell-Rabb, J. A structure-function analysis of chlorophyllase reveals a mechanism for activity regulation dependent on disulfide bonds. *J. Biol. Chem.* **2023**, *299*, 102958.
(15) Hu, X. Y.; Makita, S.; Schelbert, S.; Sano, S.; Ochiai, M.; Tsuchiya, T.; Hasegawa, S. F.; Hörtensteiner, S.; Tanaka, A.; Tanaka, R. Reexamination of Chlorophyllase Function Implies Its Involvement in Defense against Chewing Herbivores. *Plant Physiol.* **2015**, *167*, 660−670.
(16) Benedetti, C. E.; Costa, C. L.; Turcinelli, S. R.; Arruda, P. Differential expression of a novel gene in response to coronatine, methyl jasmonate, and wounding in the Coi1 mutant of Arabidopsis. *Plant Physiol.* **1998**, *116*, 1037−1042.
(17) Kariola, T.; Brader, G.; Li, J.; Palva, E. T. Chlorophyllase 1, a damage control enzyme, affects the balance between defense pathways in plants. *Plant Cell* **2005**, *17*, 282−294.
(18) Guyer, L.; Hofstetter, S. S.; Christ, B.; Lira, B. S.; Rossi, M.; Hortensteiner, S. Different mechanisms are responsible for chlorophyll dephytylation during fruit ripening and leaf senescence in tomato. *Plant Physiol.* **2014**, *166*, 44−56.
(19) Chen, L. F. O.; Lin, C. H.; Kelkar, S. M.; Chang, Y. M.; Shaw, J. F. Transgenic broccoli (Brassica oleracea var. italica.) with antisense chlorophyllase (BoCLH1) delays postharvest yellowing. *Plant Sci.* **2008**, *174*, 25−31.
(20) Jacob-Wilk, D.; Holland, D.; Goldschmidt, E. E.; Riov, J.; Eyal, Y. Chlorophyll breakdown by chlorophyllase: isolation and functional expression of the Chlase1 gene from ethylene-treated Citrus fruit and its regulation during development. *Plant J.* **1999**, *20*, 653−661.
(21) Azoulay-Shemer, T.; Harpaz-Saad, S.; Cohen-Peer, R.; Mett, A.; Spicer, V.; Lovat, N.; Krokhin, O.; Brand, A.; Gidoni, D.; Standing, K. G.; et al. Dual N- and C-Terminal Processing of Citrus Chlorophyllase Precursor Within the Plastid Membranes leads to the Mature Enzyme. *Plant Cell Physiol.* **2011**, *52*, 70−83.
(22) Tian, Y. N.; Zhong, R. H.; Wei, J. B.; Luo, H. H.; Eyal, Y.; Jin, H. L.; Wu, L. j.; Liang, K. y.; Li, Y. m.; Chen, S. z.; et al. Arabidopsis CHLOROPHYLLASE 1 protects young leaves from long-term photodamage by facilitating FtsH-mediated D1 degradation in photosystem II repair. *Mol. Plant* **2021**, *14*, 1149−1167.

(23) Liao, Y.; An, K.; Zhou, X.; Chen, W. J.; Kuai, B. K. AtCLH2, a Typical but Possibly Distinctive Chlorophyllase Gene in Arabidopsis. *J. Integr. Plant Biol.* **2007**, *49*, 531−539.
(24) Christ, B.; Hörtensteiner, S. Mechanism and Significance of Chlorophyll Breakdown. *J. Plant Growth Regul.* **2014**, *33*, 4−20.
(25) Visioli, F.; Marangoni, F.; Fogliano, V.; Del Rio, D.; Martinez, J. A.; Kuhnle, G.; Buttriss, J.; Da Costa Ribeiro, H.; Bier, D.; Poli, A. The ultra-processed foods hypothesis: a product processed well beyond the basic ingredients in the package. *Nutr. Res. Rev.* **2022**, *36*, 340−350.
(26) Fleming, P. J.; Fleming, K. G. HullRad: Fast Calculations of Folded and Disordered Protein and Nucleic Acid Hydrodynamic Properties. *Biophys. J.* **2018**, *114*, 856−869.
(27) Krissinel, E.; Henrick, K. Inference of macromolecular assemblies from crystalline state. *J. Mol. Biol.* **2007**, *372*, 774−797.
(28) Gasteiger, E.; Gattiker, A.; Hoogland, C.; Ivanyi, I.; Appel, R. D.; Bairoch, A. ExPASy: the proteomics server for in-depth protein knowledge and analysis. *Nucleic Acids Res.* **2003**, *31*, 3784−3788.
(29) Mirdita, M.; Schutze, K.; Moriwaki, Y.; Heo, L.; Ovchinnikov, S.; Steinegger, M. ColabFold: making protein folding accessible to all. *Nat. Methods* **2022**, *19*, 679−682.
(30) Jumper, J.; Evans, R.; Pritzel, A.; Green, T.; Figurnov, M.; Ronneberger, O.; Tunyasuvunakool, K.; Bates, R.; Žídek, A.; Potapenko, A.; et al. Highly accurate protein structure prediction with AlphaFold. *Nature* **2021**, *596*, 583−589.
(31) Arkus, K. A.; Cahoon, E. B.; Jez, J. M. Mechanistic analysis of wheat chlorophyllase. *Arch. Biochem. Biophys.* **2005**, *438*, 146−155.
(32) Schrag, J. D.; Cygler, M. [4] Lipases and hydrolase fold. *Methods Enzymol.* **1997**, *284*, 85−107.
(33) Capitani, G.; Markovic-Housley, Z.; DelVal, G.; Morris, M.; Jansonius, J. N.; ürmann, P. Crystal structures of two functionally different thioredoxins in spinach chloroplasts 1 1Edited by R. Huber. *J. Mol. Biol.* **2000**, *302*, 135−154.
(34) Balsera, M.; Buchanan, B. B. Evolution of the thioredoxin system as a step enabling adaptation to oxidative stress. *Free Radical Biol. Med.* **2019**, *140*, 28−35.
(35) Wolf, Y. I.; Grishin, N. V.; Koonin, E. V. Estimating the number of protein folds and families from complete genome data 1 1Edited by J. Thornton. *J. Mol. Biol.* **2000**, *299*, 897−905.
(36) Gerlt, J. A.; Babbitt, P. C. Divergent evolution of enzymatic function: mechanistically diverse superfamilies and functionally distinct suprafamilies. *Annu. Rev. Biochem.* **2001**, *70*, 209−246.
(37) Li, B.; Jo, M.; Liu, J.; Tian, J.; Canfield, R.; Bridwell-Rabb, J. Structural and mechanistic basis for redox sensing by the cyanobacterial transcription regulator RexT. *Commun. Biol.* **2022**, *5*, 275.
(38) Zhang, C.; DeLisi, C. Protein folds: molecular systematics in three dimensions Cell. *Cell. Mol. Life Sci.* **2001**, *58*, 72−79.
(39) Fraser, N. J.; Liu, J. W.; Mabbitt, P. D.; Correy, G. J.; Coppin, C. W.; Lethier, M.; Perugini, M. A.; Murphy, J. M.; Oakeshott, J. G.; Weik, M.; et al. Evolution of Protein Quaternary Structure in Response to Selective Pressure for Increased Thermostability. *J. Mol. Biol.* **2016**, *428*, 2359−2371.
(40) Rauwerdink, A.; Kazlauskas, R. J. How the Same Core Catalytic Machinery Catalyzes 17 Different Reactions: the Serine-Histidine-Aspartate Catalytic Triad of α/β-Hydrolase Fold Enzymes. *ACS Catal.* **2015**, *5*, 6153−6176.
(41) Dimitriou, P. S.; Denesyuk, A.; Takahashi, S.; Yamashita, S.; Johnson, M. S.; Nakayama, T.; Denessiouk, K. Alpha/beta-hydrolases: A unique structural motif coordinates catalytic acid residue in 40 protein fold families. *Proteins* **2017**, *85*, 1845−1855.
(42) Nardini, M.; Dijkstra, B. W. α/β Hydrolase fold enzymes: the family keeps growing. *Curr. Opin. Struct. Biol.* **1999**, *9*, 732−737.
(43) Li, Y.; Zhang, R.; Wang, C.; Forouhar, F.; Clarke, O. B.; Vorobiev, S.; Singh, S.; Montelione, G. T.; Szyperski, T.; Xu, Y.; et al. Oligomeric interactions maintain active-site structure in a non-cooperative enzyme family. *EMBO J.* **2022**, *41*, No. e108368.
(44) Levy, E. D.; Erba, E. B.; Robinson, C. V.; Teichmann, S. A. Assembly reflects evolution of protein complexes. *Nature* **2008**, *453*, 1262−1265.
(45) Robinson-Rechavi, M.; Alibes, A.; Godzik, A. Contribution of electrostatic interactions, compactness and quaternary structure to protein thermostability: lessons from structural genomics of Thermotoga maritima. *J. Mol. Biol.* **2006**, *356*, 547−557.
(46) Kumari, N.; Yadav, S. Modulation of protein oligomerization: An overview. *Prog. Biophys. Mol. Biol.* **2019**, *149*, 99−113.
(47) Liebeton, K.; Zacharias, A.; Jaeger, K. E. Disulfide bond in Pseudomonas aeruginosa lipase stabilizes the structure but is not required for interaction with its foldase. *J. Bacteriol.* **2001**, *183*, 597−603.
(48) Han, X.; Liu, W.; Huang, J. W.; Ma, J.; Zheng, Y.; Ko, T. P.; Xu, L.; Cheng, Y. S.; Chen, C. C.; Guo, R. T. Structural insight into catalytic mechanism of PET hydrolase. *Nat. Commun.* **2017**, *8*, 2106.
(49) Tournier, V.; Topham, C. M.; Gilles, A.; David, B.; Folgoas, C.; Moya-Leclair, E.; Kamionka, E.; Desrousseaux, M. L.; Texier, H.; Gavalda, S.; et al. An engineered PET depolymerase to break down and recycle plastic bottles. *Nature* **2020**, *580*, 216−219.
(50) Schafer, J. W.; Zoi, I.; Antoniou, D.; Schwartz, S. D. Optimization of the Turnover in Artificial Enzymes via Directed Evolution Results in the Coupling of Protein Dynamics to Chemistry. *J. Am. Chem. Soc.* **2019**, *141*, 10431−10439.
(51) Schwartz, S. D. Protein Dynamics and Enzymatic Catalysis. *J. Phys. Chem. B* **2023**, *127*, 2649−2660.
(52) Casadevall, G.; Pierce, C.; Guan, B.; Iglesias-Fernandez, J.; Lim, H.-Y.; Greenberg, L. R.; Walsh, M. E.; Shi, K.; Gordon, W.; Aihara, H.; et al. Designing Efficient Enzymes: Eight Predicted Mutations Convert a Hydroxynitrile Lyase into an Efficient Esterase. **2023**, bioRxiv 2023.08.23.554512.
(53) Khazim, K.; Giustarini, D.; Rossi, R.; Verkaik, D.; Cornell, J. E.; Cunningham, S. E.; Mohammad, M.; Trochta, K.; Lorenzo, C.; Folli, F.; et al. Glutathione redox potential is low and glutathionylated and cysteinylated hemoglobin levels are elevated in maintenance hemodialysis patients. *Transl. Res.* **2013**, *162*, 16−25.
(54) Aitken, C. E.; Marshall, R. A.; Puglisi, J. D. An oxygen scavenging system for improvement of dye stability in single-molecule fluorescence experiments. *Biophys. J.* **2008**, *94*, 1826−1835.
(55) Burns, J. A.; Butler, J. C.; Moran, J.; Whitesides, G. M. Selective reduction of disulfides by tris(2-carboxyethyl)phosphine. *J. Org. Chem.* **1991**, *56*, 2648−2650.
(56) Richardson, J. S.; Videau, L. L.; Williams, C. J.; Richardson, D. C. Broad Analysis of Vicinal Disulfides: Occurrences, Conformations with Cis or with Trans Peptides, and Functional Roles Including Sugar Binding. *J. Mol. Biol.* **2017**, *429*, 1321−1335.
(57) Ehira, S.; Ohmori, M. The redox-sensing transcriptional regulator RexT controls expression of thioredoxin A2 in the cyanobacterium Anabaena sp. strain PCC 7120. *J. Biol. Chem.* **2012**, *287*, 40433−40440.
(58) Richter, A. S.; Grimm, B. Thiol-based redox control of enzymes involved in the tetrapyrrole biosynthesis pathway in plants. *Front. Plant Sci.* **2013**, *4*, 371.
(59) Xie, Z.; Wu, S.; Chen, J.; Zhu, X.; Zhou, X.; Hortensteiner, S.; Ren, G.; Kuai, B. The C-terminal cysteine-rich motif of NYE1/SGR1 is indispensable for its function in chlorophyll degradation in Arabidopsis. *Plant Mol. Biol.* **2019**, *101*, 257−268.
(60) Jensen, P. E.; Reid, J. D.; Hunter, C. N. Modification of cysteine residues in the ChlI and ChlH subunits of magnesium chelatase results in enzyme inactivation. *Biochem. J.* **2000**, *352*, 435−441.
(61) Ikegami, A.; Yoshimura, N.; Motohashi, K.; Takahashi, S.; Romano, P. G.; Hisabori, T.; Takamiya, K. i.; Masuda, T. The CHLI1 subunit of Arabidopsis thaliana magnesium chelatase is a target protein of the chloroplast thioredoxin. *J. Biol. Chem.* **2007**, *282*, 19282−19291.
(62) Richter, A. S.; Wang, P.; Grimm, B. Arabidopsis Mg-Protoporphyrin IX Methyltransferase Activity and Redox Regulation Depend on Conserved Cysteines. *Plant Cell Physiol.* **2016**, *57*, 519−527.
(63) Almagro Armenteros, J. J.; Salvatore, M.; Emanuelsson, O.; Winther, O.; von Heijne, G.; Elofsson, A.; Nielsen, H. Detecting sequence signals in targeting peptides using deep learning. *Life Sci. Alliance* **2019**, *2*, No. e201900429.

https://doi.org/10.1021/acsbiomedchemau.4c00089
ACS Bio Med Chem Au 2024, 4, 353−370

(64) Liu, J. X.; Knapp, M.; Jo, M.; Dill, Z.; Bridwell-Rabb, J. Rieske Oxygenase Catalyzed C-H Bond Functionalization Reactions in Chlorophyll b Biosynthesis. *ACS Cent. Sci.* **2022**, *8*, 1393−1403.
(65) Tanaka, K.; Kakuno, T.; Yamashita, J.; Horio, T. Purification and properties of chlorophyllase from greened rye seedlings. *J. Biochem.* **1982**, *92*, 1763−1773.
(66) McFeeters, R. F.; Chichester, C. O.; Whitaker, J. R. Purification and Properties of Chlorophyllase from Ailanthus altissima (Tree-of-Heaven). *Plant Physiol.* **1971**, *47*, 609−618.
(67) Shannon, P.; Markiel, A.; Ozier, O.; Baliga, N. S.; Wang, J. T.; Ramage, D.; Amin, N.; Schwikowski, B.; Ideker, T. Cytoscape: a software environment for integrated models of biomolecular interaction networks. *Genome Res.* **2003**, *13*, 2498−2504.

https://doi.org/10.1021/acsbiomedchemau.4c00089
ACS Bio Med Chem Au 2024, 4, 353−370